Modeling Pumped Thermal Energy Storage with Waste Heat Harvesting

by

Miles L Lindsey Abarr

B.S., Aerospace Engineering

University of California San Diego, 2010

M.S., Mechanical Engineering

University of Colorado Boulder, 2013

A thesis submitted to the

Faculty of the Graduate School of the

University of Colorado in partial fulfillment

of the requirement for the degree of

Doctor of Philosophy

Department of Mechanical Engineering

2016

This thesis entitled:

Modeling Pumped Thermal Energy Storage with Waste Heat Harvesting

written by Miles L Lindsey Abarr

has been approved for the Department of Mechanical Engineering

_____

Dr. Lupita Montoya

_____

Dr. Jean Hertzberg

Date_____

The final copy of this thesis has been examined by the signatories, and we find that both the content and the form meet acceptable presentation standards of scholarly work in the above mentioned discipline.

Abarr, Miles L Lindsey (Ph.D., Mechanical Engineering)

Modeling Pumped Thermal Energy Storage with Waste Heat Harvesting

Thesis directed by Assistant Professor Lupita Montoya

This work introduces a new concept for a utility scale combined energy storage and generation system. The proposed design utilizes a pumped thermal energy storage (PTES) system, which also utilizes waste heat leaving a natural gas peaker plant. This system creates a low cost utility-scale energy storage system by leveraging this dual-functionality. This dissertation first presents a review of previous work in PTES as well as the details of the proposed integrated bottoming and energy storage system. A time-domain system model was developed in Mathworks R2016a Simscape and Simulink software to analyze this system. Validation of both the fluid state model and the thermal energy storage model are provided. The experimental results showed the average error in cumulative fluid energy between simulation and measurement was +/- 0.3% per hour. Comparison to a Finite Element Analysis (FEA) model showed <1% error for bottoming mode heat transfer.

The system model was used to conduct sensitivity analysis, baseline performance, and levelized cost of energy of a recently proposed Pumped Thermal Energy Storage and Bottoming System (Bot-PTES) that uses ammonia as the working fluid. This analysis focused on the effects of hot thermal storage utilization, system pressure, and evaporator/condenser size on the system performance. This work presents the estimated performance for a proposed baseline Bot-PTES. Results of this analysis showed that all selected parameters had significant effects on efficiency, with the evaporator/condenser size having the largest effect over the selected ranges. Results for the baseline case showed stand-alone energy storage efficiencies between 51 and 66% for varying power levels and charge states, and a stand-alone bottoming efficiency of 24%. The resulting efficiencies for this case were low compared to competing technologies; however, the dual-functionality of the Bot-PTES enables it to have higher capacity factor, leading to $91-197/MWh levelized cost of energy compared to $262-284/MWh for batteries and $172-254/MWh for Compressed Air Energy Storage.

Acknowledgements

The work presented in this dissertation has been funded by Bright Energy Storage Technologies (BEST) LLP. Thanks to Alex Lau for his investment in BEST, Scott Frazier for intellectual contributions to this work, Brendan Geels for his experimental support, Jennifer Fon Tuey for her work on Hot TES design, Bill Becker for help with system and evaporator/condenser analysis, and all other BEST employees for their work on various aspects of Bot-PTES development.

Thanks to my committee members: Dr. Lupita D. Montoya, Dr. Jean Hertzberg, Dr. Julie Steinbrenner, Dr. Conrad Stoldt, and Dr. Frank Barnes for their advice throughout my dissertation process. Special thanks to Dr. Montoya and Dr. Hertzberg for giving me extra guidance and assistance over my Ph.D. career. Also, thanks to Dr. Victor Bright for advising me during my first two years of graduate school.

Thanks to my friends and family for their encouragement over the years. Thanks to my parents for instilling in me the confidence to take on any challenge, and for all the effort it took to raise me. Lastly, thanks to my wonderful girlfriend, Lauren, for going over and beyond to support me over the past few years, and for being a consistent joy in my life.

Contents

Tables

Figures

1. Chapter 1: Introduction

Growing awareness of climate change has led to an increased interest in renewable energy technologies. Since renewable energies are inherently intermittent, however, they require energy storage systems in order to provide dispatchable grid power. Presently, the most recognized technologies for storing energy in large-scales are compressed air energy storage (CAES) and pumped hydro energy storage (PHS). CAES has been proposed in recent years as the most economically viable option for large-scale energy storage

Another approach for large-scale energy storage is Pumped Thermal Energy Storage (PTES). Though there are some variations on PTES, all proposed systems to date charge a thermal reservoir with a heat pump and discharge it via a thermal engine.

PTES combines common thermodynamic cycles that are low cost, modular, and location-independent; however, only a few research groups have pursued this form of energy storage thus far. This lack of interest is partially due to the recognized inefficiency of thermal engines for creating electricity—ranging between about 20 and 50% for most heat generation systems [1]. When a heat pump is combined with a thermal engine to create a full charge and discharge energy storage cycle, however, the system becomes more attractive.

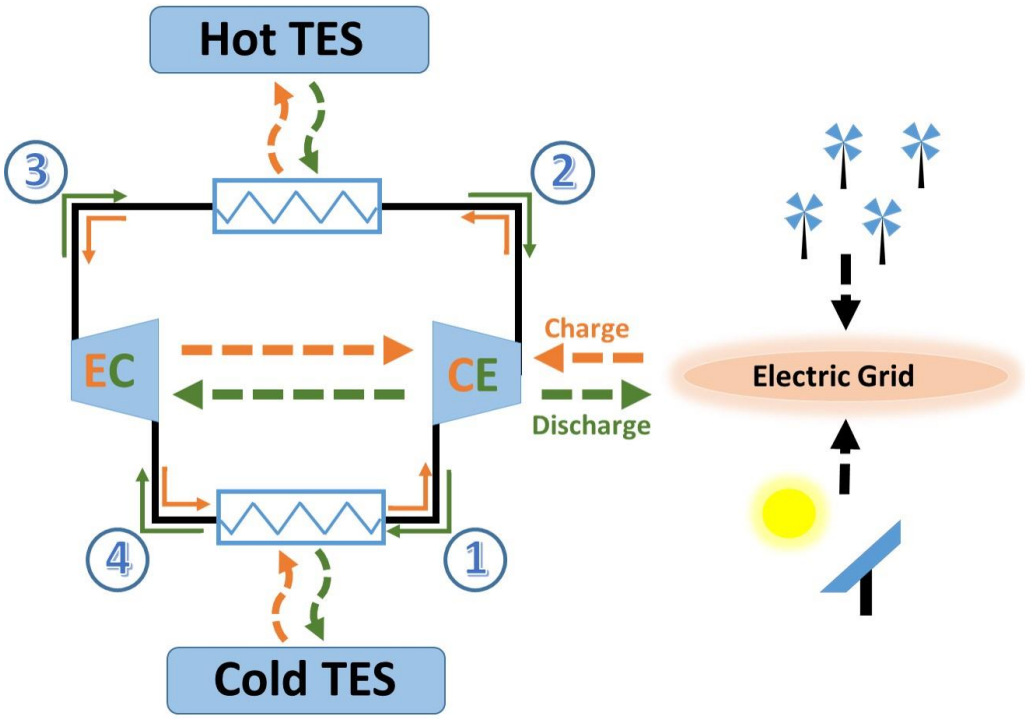

Figure 1: Generic PTES system. CE = Compressor/Expander, EC = Expander/Compressor. Energy flows are in dashed lines. Wavy lines represent heat flows. Solid lines represent fluid flows.

Figure 1 shows a generic stand-alone PTES cycle. In charge mode, shown in orange, electricity from the grid is used to run a heat pump and create a thermal potential in the system between a Hot TES and a Cold TES. First, the CE compresses a cold gas (State 1). The hot, pressurized gas (State 2) then stores heat into the Hot TES. Next, the cooled pressurized fluid (State 3) is expanded through the EC where electricity is generated to help run the hot compressor. The cold, low-pressure fluid (State 4) cools the Cold TES before the fluid re-enters the hot compressor.

In discharge mode, shown in green, a standard thermal engine cycle is used to generate electrical energy from the temperature difference (heat potential) between the Hot and Cold TES using the same equipment as in charge mode. At the end of the discharge cycle, the heat potential has been reduced, and the system is ready for charging again. Whether or not the working fluid condenses to liquid through the Cold TES determines whether the process is a Rankine-like process or a Brayton-like process. The heat storage needs and EC power levels vary

substantially between these options—each with unique pragmatic challenges, some of which will be discussed in section 2 of this paper.

Parameters	Description	Nominal Units
W	work energy	J
Q	heat energy	J
$\dot{W}$	work power	W
$\dot{Q}$	heat power	W
η	efficiency	1
ρ	density	kg/m^3
C	specific heat	J/kg/K
V	volume	m^3
T	temperature	K
t	time	s
z	Hot TES axial distance along fluid path	m
a	Xu et al. lumped cylindrical capacitance inner radius	m
b	Xu et al. lumped cylindrical capacitance outer radius	m
r	radial distance	m
h	fluid specific enthalpy	J/kg
U	overall heat transfer coefficient	$W/m^2/K$
k	conductivity	W/m/K
A	area	m^2
IR	inner radius of a lumped mass in the Hot TES	m
OR	outer radius of a lumped mass in the Hot TES	m
R	thermal resistance	K/W
L	axial length of a mass	m
$\dot{V}$	volumetric flow	m^3/s
P	pressure	Pa
φ	Hot TES utilization	1
E	energy state	J
Superscripts		
Dis	discharge operation	
Ch	charge operation	
*	adjusted	
Bot	bottoming operation	
Subscripts		
ES	energy storage	
Tot	total	
CE	vapor compressor/expander	
EC	liquid expander/compressor	

Hot	hot, high pressure side of the system	
Cold	cold, low pressure side of the system	
LM	Hot TES lumped mass	
eff	Hot TES effective parameter	
f	Hot TES fluid	
conv	Hot TES fluid convective	
tube	Hot TES tubing	
WF	Hot TES working fluid	
cyl	cylinder	
SS	steady state mode, referring to bottoming operation	
Exh	exhaust	
actual	actual simulated value, after corrections for expected isentropic efficiencies	
1	working fluid state at low pressure side of the CE	
2	working fluid state at high pressure side of the CE	
3	working fluid state at high pressure side of EC	
4	working fluid state at low pressure side of EC	
$\bar{s}$	isentropic process	
electric	electric energy	
mech	mechanical	
gen	generator	
motor	motor	
cTES	Cold TES	
fan	evaporator/condenser (Cold TES) fan	
FCS	fully charged state	
FDS	fully discharged state	
ref	reference	
Bot	bottoming operation	
Available	energy available	

Table 1: Nomenclature used for equations and system parameters.

Thermal engines are fundamentally inefficient because heat must be rejected to a cold reservoir, and not used to produce work, as dictated by the second law of thermodynamics. In this proposed combined system, however, *the heat rejected to storage (Cold TES) during the thermal engine cycle (discharge phase) is then used during the charge phase*. Thus, although the charge and discharge cycles are individually subject to Carnot efficiency limits, when combined sequentially there is no theoretical limit placed on the *round-trip efficiency* (η_{ES}) of a PTES. Theoretically, an ideal system (neglecting heat transfer and mechanical inefficiencies) can be 100% efficient. This can be shown as follows:

$$\eta_{ES} = \frac{W_{Tot}^{Dis}}{W_{Tot}^{Ch}} \tag{1.1}$$

where W_{Tot}^{Dis} is the total electric energy generated during the discharge cycle (thermal engine), and W_{Tot}^{Ch} is the total electric energy consumed during the charge cycle (heat pump). Table 1 includes all of the nomenclature used for system parameters and equations used throughout this paper. Since

$$W_{Tot}^{Ch} = W_{CE}^{Ch} - W_{EC}^{Ch} \tag{1.2}$$

where W_{CE}^{Ch} is the compression work and W_{EC}^{Ch} is the re-expansion work done during the heat pump cycle,

$$W_{CE}^{Ch} - W_{EC}^{Ch} = Q_{Hot}^{Ch} - Q_{Cold}^{Ch} \tag{1.3}$$

and Q_{HotTES}^{Ch} and $Q_{ColdTES}^{Ch}$ are the heat transferred to the hot storage and taken from the cold storage, respectively, during the heat pump cycle. Furthermore,

$$W_{Tot}^{Dis} = W_{CE}^{Dis} - W_{EC}^{Dis} \tag{1.4}$$

where W_{CE}^{Dis} is the expansion work and W_{EC}^{Dis} is the pressurization work done during the discharge cycle. This total thermal engine work is also equal to

$$W_{CE}^{Dis} - W_{EC}^{Dis} = Q_{Hot}^{Dis} - Q_{Cold}^{Dis} \tag{1.5}$$

where Q_{Hot}^{Dis} and Q_{Cold}^{Dis} are the heat transferred from the hot storage and to the cold storage, respectively, during the thermal engine cycle. Combining these equations leads to:

$$\eta_{ES} = \frac{Q_{Hot}^{Dis} - Q_{Cold}^{Dis}}{Q_{Hot}^{Ch} - Q_{Cold}^{Ch}} \quad (1.6)$$

Consequently, if the heat transfers during the heat pump cycle are equivalent to those during the thermal engine cycle (i.e., there are no irreversibilities or heat loss), there can be theoretically 100% energy storage efficiency for the entire PTES process. In reality, there are irreversibilities of heat transfer and mechanical components, as well as economic practicalities that must be factored in to predict a realistic round-trip efficiency and system cost.

A unique feature of PTES is that since it uses heat to generate electricity in the discharge cycle, heat can also be harvested with the system. Therefore, PTES can perform as an energy generation device and a storage device with the same set of equipment. This dual-functionality can lead to lower effective capital costs and/or higher integrated energy efficiencies.

This paper proposes a bottoming system with PTES (Bot-PTES). The bottoming system is designed to use waste heat rejected by a natural gas peaker plant, assuming there is no steam bottoming system already in place. This is a common situation, as natural gas peaker plants are typically put in place as a single-cycle (no bottoming cycle) system. The Bot-PTES system can store energy (in the form of heat generated by electricity) from renewable sources such as wind or solar, and load shift the fossil fuel heat as desired.

The objective of this work was to conduct an initial analysis for this proposed Bot-PTES system. A time-domain model was developed, which can handle the transient effects inherent in storing heat. While previous work has investigated various stand-alone PTES systems, to the authors' knowledge, none have analyzed a PTES integrated with another heat source. The integration of these systems offers advantages that have not been properly explored and merit some study. The objective of this work was to investigate this potential synergy.

The analysis of this system is divided into two papers, Part A and Part B. Part A gives the background on PTES, explanation of the Bot-PTES concept, and description of the modeling methods for the Bot-PTES system. Part B includes a parametric analysis of key system factors, and then gives a baseline design system performance, including expected cost and efficiency.

2. Chapter 2: Bot-PTES Concept and Model

2.1. Background

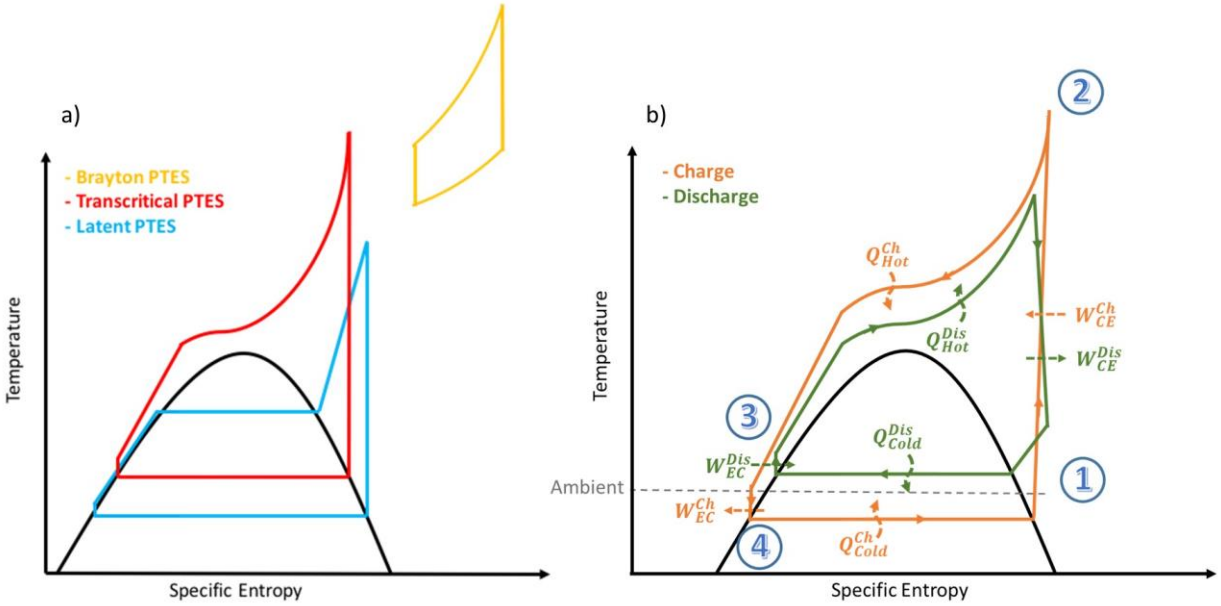

Figure 2: a) Generic T-s diagram for ideal Brayton PTES, Transcritical PTES, and Latent PTES cycle, and b) Non-ideal Transcritical PTES charge and discharge cycles.

The first PTES concepts were proposed in 1924 and 1933 [2], [3] and by 1978, patents had been granted [4,5]. There have been other patents granted for PTES concepts since the 1970s [4–15] and most of them were awarded outside the US. They all appear to be variations of a generalized PTES system, with various TES materials and working fluids (WF), each exhibiting unique technical challenges.

Currently, the literature shows three main subcategories for PTES: 1) Brayton PTES 2) Transcritical PTES, and 3) Latent PTES. Figure 2 shows: (a) all three ideal cycles on a T-s diagram and (b) non-ideal Transcritical PTES charge and discharge cycles. The main trade-off for all types of PTES is between the back-work ratio and the heat storage ratio. The back work ratio is the amount of re-expansion work relative to the compression work performed during the charge mode (W_{EC}^{Ch}/W_{CE}^{Ch}). The heat storage ratio is the amount of heat stored in the Hot TES relative to the compression work in the charge mode (Q_{Hot}^{Ch}/W_{CE}^{Ch}). Higher back-work ratio requires

purchasing more machinery, and the machinery efficiencies have more weight on system efficiency. For example, Kim et al. showed that for Brayton PTES with machine efficiencies equal to 90%, and a back-work ratio of 0.5, the maximum possible PTES system efficiency was only about 55% [16]. Conversely, higher heat storage ratio requires purchasing more thermal energy storage, and the thermal energy storage heat transfer performance has more weight on system efficiency.

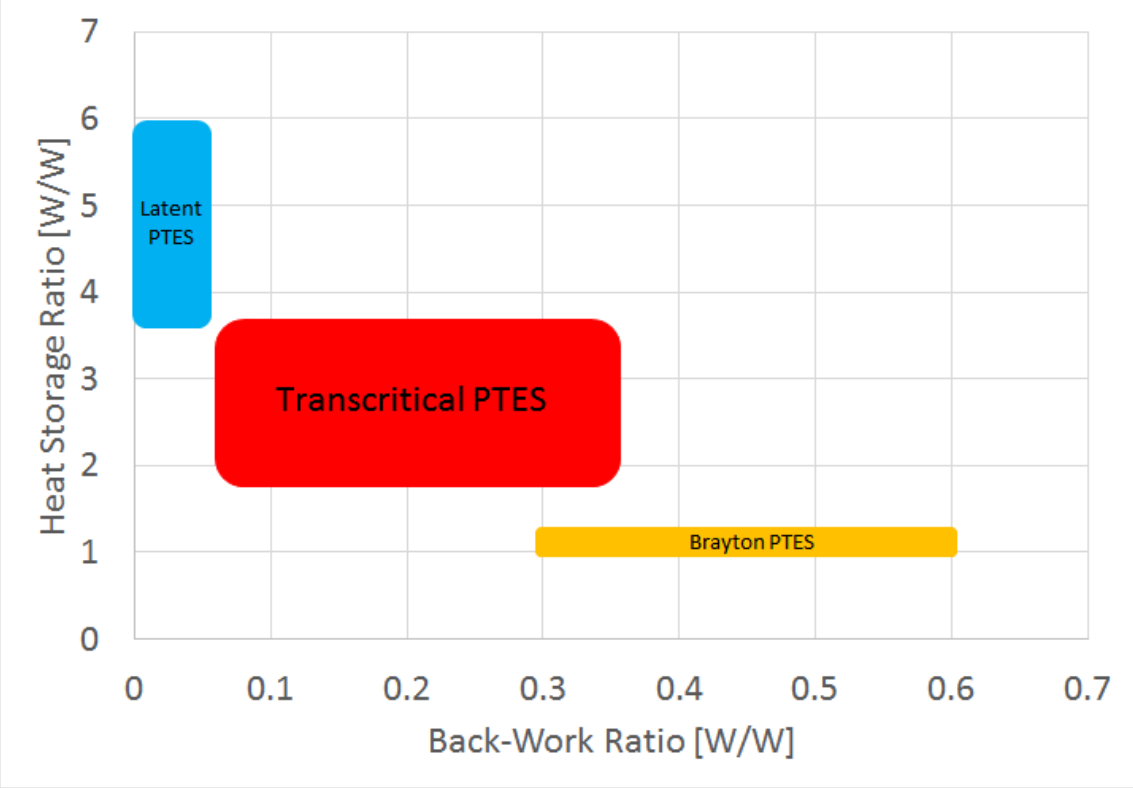

Figure 3: Comparison for different PTES types based on ideal cycle analysis. Commonly considered working fluids for PTES were used to derive these numbers, such as argon, air, water, CO2, and ammonia.

Figure 3 shows how the different PTES forms compare with regard to back work ratio and heat storage ratio, which are inversely related. While Brayton PTES tends to have the highest back-work ratio and the lowest heat storage ratio, the Latent PTES has the lowest back-work ratio and the highest heat storage ratio. The system considered for this work utilizes a Transcritical PTES system.

2.1.1.Brayton PTES

The Brayton PTES resembles a Brayton Cycle thermal engine and it uses a vapor-phase WF for the entire cycle. Brayton PTES may have both a hot and a cold TES. In the charge mode, the WF absorbs heat from the cold TES before it enters a compressor where sensible heat and pressure are added to the fluid. The WF then rejects heat to the hot TES before being expanded by a turbine and repeating the cycle. This is the heat pump portion of the energy storage cycle where electricity is used (stored) to heat the hot TES and cool the cold TES, creating a thermodynamic potential between the two TES's.

In discharge mode, the reverse happens where the WF under high pressure absorbs heat from the hot TES before being expanded by a turbine and rejecting heat to the cold TES. The fluid is then compressed to high pressure again before repeating the cycle. This is the thermal engine portion of the energy storage cycle where the thermodynamic potential stored during the heat pump phase is used to produce a net electric output.

The advantage of Brayton PTES is that both the hot and cold heat transfers are purely sensible heat. This is advantageous because the latent energy of the WF does not need to be stored, leading to a smaller sized hot and cold TES. The main drawback of this storage is a high back-work ratio during charge and discharge (Figure 4). For example, with charge mode the expander supplies a large portion of the work for the cycle. This leads to the requirement for not only a larger EC, but also more efficient machinery in general. The reason the machinery must be more efficient, is because more energy must flow through the machinery per net energy into or out of the system. Figure 4 demonstrates how important compressor and expander machine efficiencies become with increasing back-work ratio. The graph shows the maximum possible efficiency achievable, that is, assuming no other losses in the system, when considering only the overall efficiency of the machinery. For example, with machine efficiencies equal to 90%, and a back-work ratio of 0.5, the maximum possible PTES system efficiency is only approximately 55%. Once heat transfer effects and auxiliary losses are added to the system, the efficiency will then become worse.

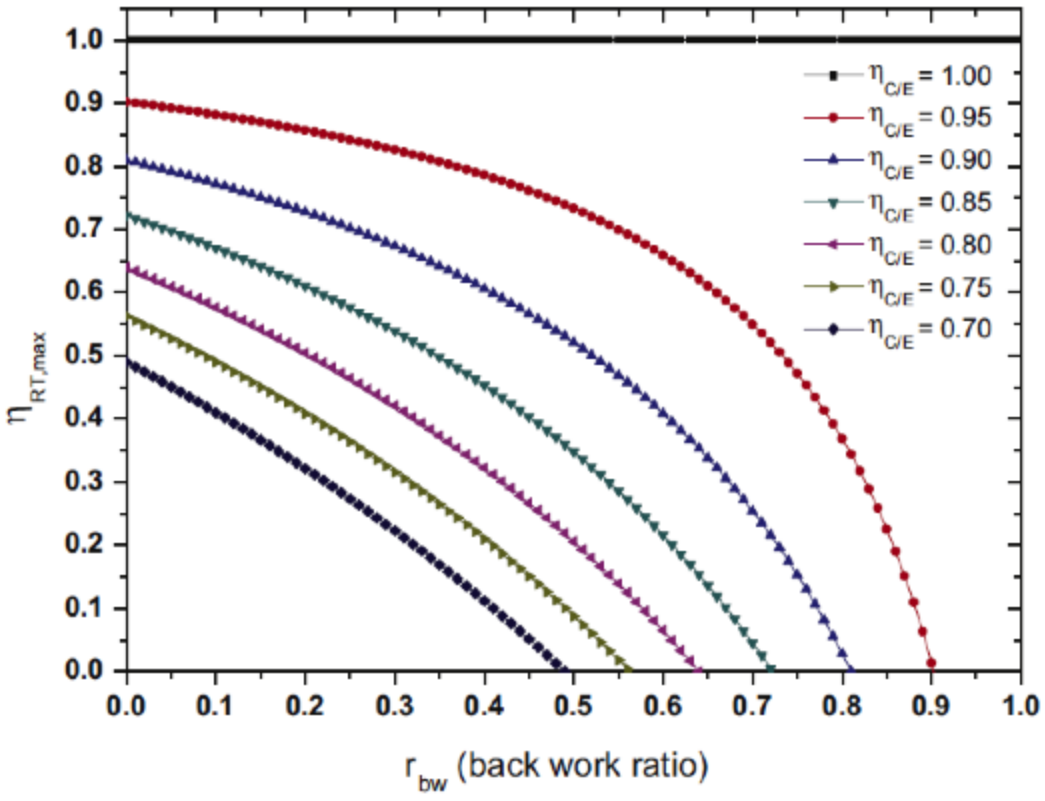

Figure 4: Figure from Kim et al. showing the effective of back-work ratio on maximum round-trip efficiency ($\eta_{RT,max}$) for varying compressor and expander efficiencies ($\eta_{C/E}$) [16].

Desrues et al. presented one of the first PTES systems in the recent literature [17]. They outlined the thermodynamic analysis for such a process, as well as irreversible effects of using a refractory material TES for both the hot and cold side. Their conceptual TES largely resembles a rock bed storage system. Their analysis showed that it took about 7 charge/discharge cycles before the TES steadied out to a constant amount of energy storage. That is, the thermal gradients within the TES drift during the first few cycles of charge/discharge, until the TES converges to a desired spatial temperature gradient, and therefore total energy within it. Using estimated losses through the turbo-machinery, Desrues et al. showed a possible round-trip efficiency of 66.7%, which includes all expected irreversibilities.

Howes et al. focused on the development of high efficiency compressors and expanders for a Brayton PTES system [18]. He focused on low pressure-drop valves, as pressure-drop in a

Brayton PTES has large implications for exergy loss. Once again, this comes back to the high back-work ratio needed with Brayton PTES. Howes predicted 72% round-trip efficiency for his system, with capital costs of only $470/kW plus a marginal energy cost of $17/kWh.

2.1.2.Latent PTES

Latent PTES involves a latent transition on the hot and cold sides of the cycle. In charge mode, liquid is evaporated by a low temperature TES. The saturated vapor is then compressed. The hot, pressurized gas gives up its energy to the hot TES until it condenses and cools back to the cold TES entropy before it is throttled or expanded to the initial temperature and pressure, and the cycle repeats. In discharge mode, the reverse happens: the cool low-pressure liquid is first pumped to a high pressure before it enters the hot TES to be heated and evaporated. The hot pressurized gas is then expanded to the saturated vapor point and condensed by the cold TES.

The advantage of Latent PTES is that it has a low back-work ratio. In the charge mode, there is relatively little work gained by expanding the liquid back to low pressure, and the same goes for the pumping work required in discharge. This lessens the requirement for highly efficient compressors and expanders. The main drawback of Latent PTES is that it has the largest heat storage ratio of any of the PTES system types. Therefore, the TES costs will be the highest for Latent PTES.

To date, only one published study has considered Latent PTES. In 2014, Steinmann proposed multiple variations of an Latent PTES system [19]. All variations considered water or multiple stages of water and ammonia as WFs. Systems kept the maximum operating temperature under 673K so that many common materials may be used. All of the systems considered in the study used a phase change material (PCM) hot TES to match the phase change of the WF. This Latent PTES study also considered the integration of a Latent PTES with other heat sources, such as solar-thermal or waste heat to enable a higher effective round-trip efficiency.

On the cold side, Steinmann proposed using the environment as the cold TES. The environment in this case could be ambient air, or some kind of water reservoir such as a lake or pond, similar to typical condensers for a steam plant. The advantages are that it is self-

stabilizing. That is, with a conventional PTES system, which uses thermally isolated hot and cold TES, there is typically a net heat increase in the system due to irreversibilities. This requires an additional system component that rejects heat to the environment. Moreover, when using an additional thermal source such as waste heat to increase hot TES energy the system requires even more net heat rejection.

Another potential advantage is that if the system is charged when the environment is hot (daytime typically) as would occur if the system is using photovoltaic (PV) power, and discharged when the environment is cold (nighttime typically), it can use the environment as an effective heat pump to improve efficiency. Specifically, when the environment is hotter during charge, this allows the system to absorb more heat during the evaporation portion of the cycle. Then in discharge, when the environment is colder, the system doesn't have to reject as much heat to condense. This leads to a net positive energy increase in the system relative to a constant temperature environment.

The main disadvantage of using the environment as the cold TES is that it is unpredictable, which increases complexity of how to run the system. Furthermore, if the system is charged when the environment is cold and discharges when it is hot, this can have the opposite effect described above, which hurts efficiency. However, if the system is using photovoltaic (PV) power to charge, then the natural charge/discharge cycle will work in this system's favor.

2.1.3.Transcritical PTES

Transcritical PTES is similar to Latent PTES, except the saturated vapor is compressed to a supercritical state. This cycle does not need a hot phase change material TES; however, it does still have a high heat storage ratio and therefore requires a large hot and cold TES. It also generally requires a higher-pressure system to reach supercritical conditions.

All of the published Transcritical PTES concepts use carbon dioxide (CO_2) as the working fluid, sensible liquid water as the hot TES, and liquid-to-solid water (ice) as the cold TES. This WF and hot and cold TES are environmentally benign, non-toxic, commonly used. They also have good thermal properties and are well matched in terms of operational temperatures and pressures.

In 2011, Jaroslav et al. proposed a CO_2 transcritical PTES concept [20] using off-the-shelf equipment for a pilot-scale proof-of-concept plant. The team also presented a plan and timeline for improved efficiency and cost using custom components.

Mercongoez et al. (2012) proposed some specific design attributes for a Transcritical PTES system based on the overall concept proposed by Jaroslav et al. [21]. The selected WF and TES types were the same. This team found that there is little improvement in efficiency for high temperatures above 673K. Instead, significant improvements can be achieved by lowering the low temperature using ice storage on the cold side. Mercongoez et al. (2012) also proposed a pilot plant with off-the-shelf turbomachinery, which should be able to achieve 51% round-trip efficiency. They claimed that using custom components could raise the system efficiency up to 65%.

Also in 2012, Morandin et al. presented a thermodynamic design optimization for a base case as well as alternative approaches in two papers using pinch analysis [22,23]. One of the most significant findings was that system efficiency was improved by superheating the WF prior to compression in the charge mode using recuperated heat leaving the hot TES. This step allowed high temperatures to be stored in the TES, which enabled higher output in the thermal engine mode during discharge that more than compensates for the higher compression work during charge. They admit in these papers that further techno-economic analysis is needed to prove the best cost-effective design.

In 2013, Morandin et al. conducted a thermoeconomic design optimization of their PTES concepts using transcritical CO_2. They used a genetic algorithm as their optimization solver with cost functions estimations built on vendor quotations for system components. This study found that the most sensitive design parameters are the system cycle pressures and the number of intermediate hot water storage vessels on the hot TES side.

In 2013, Fauci et al. revealed plans for the construction of the first PTES pilot plant in Zurich [24]. The plant was planned to be 5MWe with six hours of charging and 3 hours of discharging. The maximum round-trip efficiency was expected to be 40-45%. The proposed working fluid was CO_2 operated between 30 and 140 bar. The proposed hot TES storage temperature was 393K, while the cold TES storage temperature was 273K. They proposed

eventual integration of the PTES system with the district heating system to improve overall efficiency.

2.1.4.Bottoming Cycles

Bottoming cycles are cycles that utilize waste heat from another system/cycle. Bottoming cycles are relevant to this dissertation, because the proposed system will be combining bottoming functionality and PTES functionality into a single system. The point of bottoming cycles is to increase the overall work output (efficiency) from a given heat source. The most common bottoming cycle in existence is the steam Rankine cycle [1,25–27], where a steam cycle takes heat leaving a natural gas turbine and converts the heat into work.

Some other commonly investigated bottoming cycles include Rankine cycles with other working fluids, such as organic refrigerants and/or mixed refrigerants [28,29]. Others, such as the Goswami cycle, produces refrigeration in addition to a work output, and the Trilateral Flash cycle, which expands the pressurized WF as saturated liquid rather than vapor [30,31]. These cycles are not covered in this report, as they are either designed for too specific of applications, for too low grade of heat, or for special machinery.

The steam Rankine cycle has been around for well over a century and has been continuously re-optimized and re-designed to improve its efficiency. One of the more common ways to improve efficiency is to use multiple stage steam turbine expansion, where after the first stage of expansion there is a reheat process [1] to effectively capture more heat overall. Another common efficiency improvement is to use supercritical steam. This increases the pressures and temperatures of the steam to raise the Carnot limit. It also creates a better enthalpy flow match with the heat source to mitigate losses related to the pinch point of the two streams.

The Kalina cycle has been proposed as a replacement for the high temperature steam Rankine cycle. Mlcak wrote an overview of the Kalina cycle, stating that it could improve efficiency over the traditional steam Rankine cycle by 20-50% [29]. The Kalina cycle is a Rankine cycle that uses as WF a mixture of ammonia and water. Mlcak reviewed how the mixture mass fractions could be tailored to meet the application. Moreover, when using a mixture of

ammonia and water, the phase change process for the WF occurs at variable temperature, which helps match the sensible nature of the source fluid on both the evaporation side (e.g. exhaust gas heat) and the condensation side (e.g. ambient air). Moreover, it allows for recuperating some of the condensation heat by using some of that heat to preheat the pressurized WF before exchanging heat with the hot temperature source.

Research on bottoming cycles is directly applicable to the work in this paper. If a PTES cycle can be designed such that the WF and high temperature/pressure of the system aligns well with a waste heat source, the system can be used for both PTES and bottoming, which is the core of the Bot-PTES concept. The additional heat source allows for more energy output than the system would normally get with a simple charge and discharge cycle—leading to higher efficiency and capacity factor.

2.2. Proposed System Description: Bottoming with PTES

A simplified schematic of the proposed Bot-PTES system is shown in Figure 5. This Bot-PTES system is designed to be part of a natural gas combined cycle (NGCC) power plant in place of a steam system, which would normally be the bottoming system used for such a plant.

In this design it is assumed that reciprocating compressors/expanders (CE and EC) will be used rather than turbomachinery because they show promise for lowering the cost per unit power [18]. The cycle uses ammonia as the WF, a Hot TES structure made of tube-in-concrete, and a Cold TES made of an evaporator/condenser exchanging heat with ambient air. The ammonia is compressed to supercritical pressures in this cycle; therefore, it is a Transcritical PTES system design. An overlay of additional heat from a turbine exhaust (red arrow) is pumped through separate channels in the concrete Hot TES to allow for bottoming functionality with the PTES system. The system configuration for the present analysis was kept simple with no reheats. The cycle may have multiple stages of adiabatic compression/expansion depending on the design of the compressors/expanders.

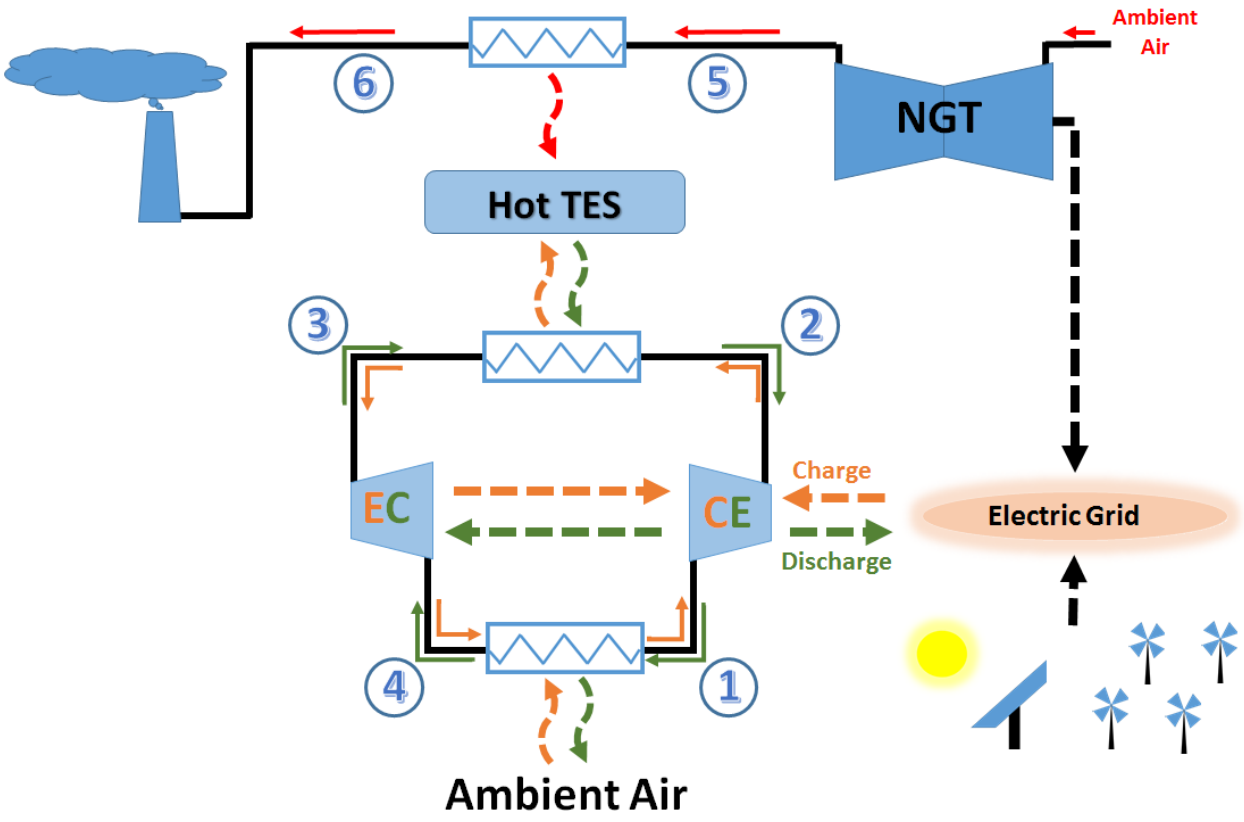

Figure 5: Simplified schematic of Bot-PTES system connected to a natural gas turbine (NGT) powered plant.

Next, we describe the rationale for selecting ammonia as the working fluid and the Hot and Cold TES designs.

2.2.1. Ammonia

Ammonia was selected as the nominal working fluid because it has good thermodynamic properties for the proposed cycle. Notably, the saturated vapor density of ammonia is high near room temperature (5.7kg/m^3 for ammonia vs 0.013kg/m^3 for steam at 288K); its specific heat ratio is also relatively high compared to other refrigerants. These factors are important for keeping the power density up (capital costs down) when using reciprocating machines. While increasing the density increases the mass flow for a constant volumetric displacement, the higher specific heat ratio leads to higher pressures and temperatures for a given compression ratio. Together, this leads to increased power density for the reciprocating

machines. Additionally, ammonia can reach high temperatures to utilize heat from the natural gas turbine exhaust, which most common refrigerants outside of steam cannot achieve. Ammonia continues to be used in large refrigeration systems under industrial guidelines like ASHRAE 15 and IIAR-2b. Also, ammonia is readily used at power plants in catalytic reduction for flue gas cleanup [32].

2.2.2. Tube-in-Concrete Hot TES

The German Aerospace Center (DLR) is a leading research facility investigating TES technologies and it has proposed several novel TES concepts (e.g., sensible, latent, and thermochemical) [33]. One robust and cost effective TES concept is their tube-in-concrete design, which was tested for approximately 13,000 hours at temperatures between 473K and 673K. Testing results showed no degradation in performance. Concrete has been proposed by other research groups as a low-cost, high-temperature, robust energy storage material [34–41].

Wu et al. studied the performance of four TES concrete structures, including those illustrated in Figure 6 [37]. Results showed that the packed-bed structure (Figure 6b) had the highest efficiency (~85-95%), while the channel-embedded structure (Figure 6a) had the lowest efficiency (~20-75%). Strasser et al. (2014) also found the packed-bed structure to be 8.37% more efficient than the structured concrete with embedded channels [41]. Nevertheless, Strasser et al. determined that the thermal ratcheting of the tank walls in the packed-bed design negatively impacted TES lifetime and reliability; therefore, they favored the structured concrete design. Other research groups have also found thermal ratcheting of the tank walls of packed-bed TES to be a significant impediment to utilizing this technology [36,42,43].

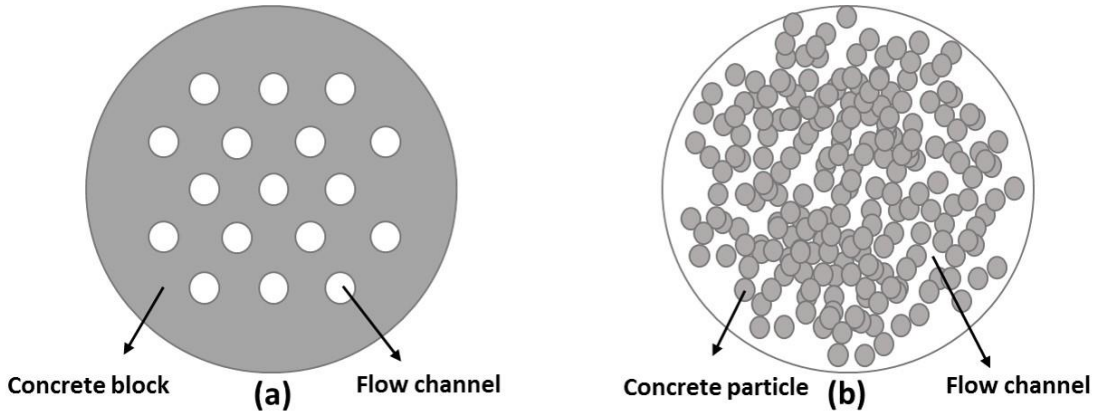

Figure 6: Two concrete (solid-state) TES structures: (a) channel-embedded, and (b) packed-bed [37].

A tube-in-concrete Hot TES was selected for the proposed Bot-PTES system because it offers advantages in terms of cost, robustness, and reliability. The proposed design here uses tubes cased into a concrete structure, as shown in the channel-embedded structure of Figure 6a.

The proposed cycle requires that the Hot TES exchange heat between two fluids—the natural gas exhaust and the working fluid—each in its own set of channels. The tube-in-concrete structure allows easy coupling of the two working fluids into the same TES.

Lastly, the working fluid must be under high pressure (over 11.3MPa required for supercritical ammonia), which is expensive for large flow areas (e.g. pressure vessels or large diameter tubing). The tube-in-concrete structure allows the use of small diameter (< 1/2”), high-pressure tubing as the containment for the working fluid rather than a pressure vessel, like a rock tank storage (i.e., packed-bed structure).

2.2.3. Air-Cooled Evaporator/Condenser Cold TES

The operation of the proposed bottoming Bot-PTES system requires a heat rejection on the cold end. Using a Cold TES instead of heat rejection would lead to heat build-up in the unit and eventually render it inoperable.

Bottoming systems using a water-cooled evaporator/condenser are common and they produce significantly better performance than air-cooled condensers. Artificial ponds are also used but they increase the overall footprint of the system. To minimize its footprint and to

avoid environmental impacts on rivers or lakes, the proposed cycle used an air-cooled evaporator/condenser.

2.3. Modeling Description for Proposed Bot-PTES System

A detailed model has been developed for all components of the proposed Bot-PTES system using the following standard assumptions:

1. Negligible heat conduction in the TES in the axial direction
2. Negligible heat transfer in the fluid in the axial direction.
3. Uniform material properties throughout the TES (the pipe lumped mass is merged into the lumped mass of the concrete).
4. Steady state flow conditions across all components.
5. Negligible pressure drop through pipes and tubing.

2.3.1. Model Overview

Mathworks R2016a software, including Matlab, Simulink, and Simscape, were used to model the proposed Bot-PTES system. Matlab was used for pre-processing of the model parameters and post-processing of the simulation data. Simulink and Simscape were used together to build a time-domain simulation for studying the effects of transient variations in the Hot TES temperature gradients. Simscape uses an acausal solver environment, which does not have specified input-output relationships. Instead, bi-directional relationships among variables are constructed through equations of physical laws. This modeling approach is preferred for building complex physical models.

While acausal modeling facilitates complex physical modeling, it can be prone to simulation failures such as unsolvable systems of equations or non-convergent solutions. To help avoid such failures but still reflect the physical complexity of the model, only the main transient component of the system, the Hot TES, was developed with Simscape. The rest of the components were modeled using Simulink, a traditional input-output modeling environment. All components were connected in a hybridized Simulink/Simscape full system model.

To model the Hot TES, a real-fluid domain was developed in Simscape and used alongside the stock Thermal Domain built into Mathworks. This custom Simscape domain accessed fluid properties from NIST REFPROP (version 9.1) and CoolProp (version 5.1.2) to calculate fluid state changes based on energy flows. The model neglected the effects of pressure drop and density changes, and therefore, the mass and pressure dynamics of the system were not considered. In other words, steady-state thermodynamic assumptions were used to determine the changes in the fluid states. Adding the mass and pressure dynamics would increase the complexity of the system of equations and negatively impact the solver robustness, slowing simulations and causing frequent simulation failures. Modeling real fluid flows with mass/pressure dynamics can lead to a system of equations with no solution (a numerical artifact) [44–46]; therefore, neglecting these dynamics in this study was deemed appropriate since the goal was only to study the high-level design and expected system efficiencies. While the mass/pressure dynamics would have an impact on the results, these effects should be small when operating a design with low system pressure drops and at steady-state conditions.

The rest of the system components were modeled in Simulink, also using pre-built fluid property tables. Compression and expansion processes were first modeled as isentropic, and then adjusted based on estimated efficiencies.

2.3.2. Hot TES Model

The proposed Bot-PTES system used a tube-in-concrete design for the Hot TES. In order to model the heat transfer throughout the Hot TES, two different modes were developed: 1) energy storage mode, and 2) bottoming mode.

The TES model was connected to the larger system model in a closed loop. The states of the working fluid entering the TES were the model outputs from the machinery components, which will be discussed next. In charge mode, the CE provided compressed fluid to the hot side of the Hot TES (Figure 5, State 2), while in discharge the EC pumped fluid to the cold side of the Hot TES (Figure 5, State 3).

The states of the exhaust fluid entering the TES were assumed to be constant at all points in time that the peaker plant was running. The exhaust fluid was modeled as air for simplification, and the heat was always directed into the high temperature side of the Hot TES.

2.3.2.1. Energy Storage Mode

When storing and retrieving energy from a solid storage medium, the heat transfer process is inherently transient—the temperature gradients are always changing. This process is challenging to model because steady-state conduction methods cannot be used. A radially discretized lumped mass modeling approach could capture the transient nature of this heat exchange; however, a modification of the method developed by Xu et al. [47] was used instead. This method is based on a single lumped mass and analyzes the energy storage in a channel-embedded structure with a large Biot number as follows:

$$\rho_{\mathrm{LM}} C_{\mathrm{LM}} V_{\mathrm{LM}} \left(\frac{\partial T_{\mathrm{LM}}}{\partial t}\right) = -U_{\mathrm{eff}} A_{eff} (T_{\mathrm{LM}} - T_{\mathrm{f}}) \tag{2.1}$$

$$\dot{m}\big(h(z_{\mathrm{out}}) - h(z_{\mathrm{in}})\big) = U_{\mathrm{eff}} A_{eff} (T_{\mathrm{LM}} - T_{\mathrm{f}}) \tag{2.2}$$

$$U_{\mathrm{eff}} = \frac{1}{\frac{1}{U_{\mathrm{conv}}} + \frac{1}{k_{LM}} \frac{a^3(4b^2 - a^2) + ab^4\left(4\mathrm{Ln}\left[\frac{b}{a}\right] - 3\right)}{4(b^2 - a^2)^2}} \tag{2.3}$$

$$A_{eff} = \frac{V_{\mathrm{LM}}}{\left(\frac{b^2 - a^2}{2a}\right)} \tag{2.4}$$

where T_{LM} is the temperature of the lumped mass of the Hot TES, T_{f} is the temperature of the fluid, ρ_{LM} is the density of the Hot TES material, C_{LM} is the specific heat capacity of the Hot TES material, V_{LM} is the volume of the Hot TES lumped mass, $\dot{m}$ is the mass flow rate of the working fluid, $h(z_{\mathrm{in}})$ and $h(z_{\mathrm{out}})$ are the specific enthalpies of the fluid at entering and leaving the lumped mass, respectively, A_{eff} is the effective area defined by Xu et al., and U_{eff} is the effective heat transfer coefficient defined by Xu et al. [47]. To define U_{eff}, the dimensions of the

lumped mass along with the fluid's convective heat transfer coefficient, $\mathrm{h_{conv}}$, and the conductivity of the lumped mass, k_{LM}, were used. Figure 7a shows the dimensions of the model by Xu et al. [47].

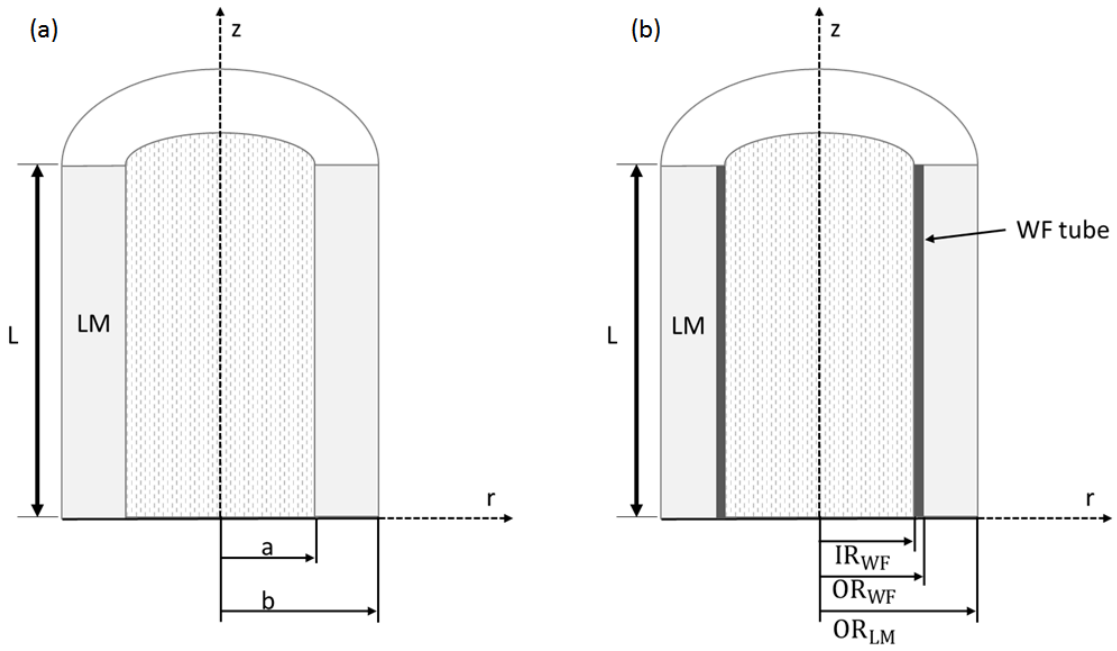

Figure 7: Schematics of (a) lumped mass model from Xu et al. and (b) a modified version of that model that includes an additional tube mass.

For the proposed Bot-PTES model, an additional lumped mass in the radial direction (Figure 7b) was added to the model by Xu et al. This modification improved its accuracy since the Bot-PTES Hot TES includes carbon steel tubing, which has significantly different material properties from concrete. Steel tubing has 1-2 orders of magnitude higher conductivity than concrete and much smaller thickness than the concrete. These differences led to a small thermal resistance of the steel conduction ($\mathrm{k}_{tube_{WF}}$) relative to the concrete conduction.

The steel conductivity term replaced the fluid convection term at the interface of the steel and concrete, while the fluid convection was dealt with explicitly. Specifically, in the overall heat transfer coefficient calculation, the $\frac{1}{\mathrm{U_{conv}}}$ became $\frac{ln(\mathrm{OR_{WF}}/\mathrm{IR_{WF}})*\mathrm{OR_{WF}}}{\mathrm{k}_{tube_{WF}}}$, based on a

steady state conductive resistance across the cylindrical pipe at the interface of the outer pipe radius and the inner concrete sleeve radius.

$$U_{eff}^{*} = \frac{1}{\frac{ln(\mathrm{OR_{WF}}/\mathrm{IR_{WF}})*\mathrm{OR_{WF}}}{\mathrm{k}_{tube_{WF}}} + \frac{1}{\mathrm{k}_{LM}} \frac{\mathrm{OR_{WF}}^{3}\left(4\mathrm{OR_{LM}}^{2} - \mathrm{OR_{WF}}^{2}\right) + \mathrm{OR_{WF}}\mathrm{OR_{LM}}^{4}\left(4\mathrm{Ln}\left[\frac{\mathrm{OR_{LM}}}{OR_{WF}}\right] - 3\right)}{4\left(\mathrm{OR_{LM}}^{2} - OR_{WF}^{2}\right)^{2}}} \tag{2.5}$$

$$A_{eff}^{*} = \frac{\mathrm{V_{LM}}}{\left(\frac{\mathrm{OR_{LM}}^{2} - \mathrm{OR_{WF}}^{2}}{2\mathrm{OR_{WF}}}\right)} \tag{2.6}$$

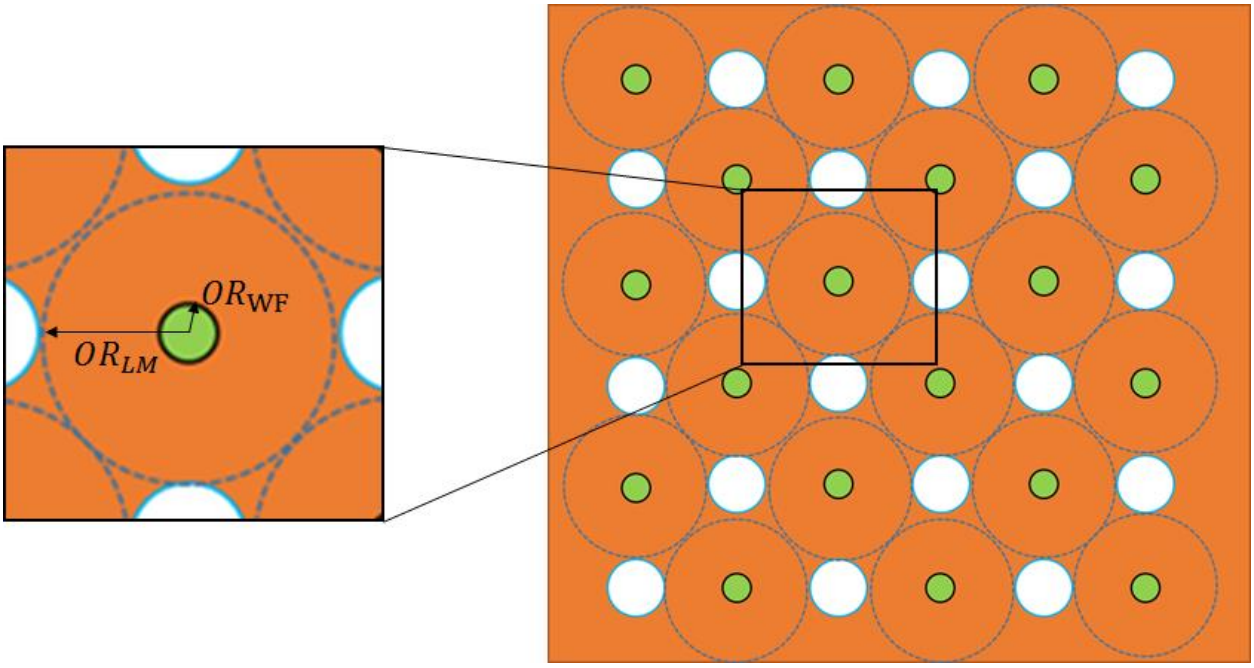

Figure 8: Visualization of lumped mass sleeves (face view) for heat transfer analysis in energy storage mode. The green circles represent the working fluid tubes, while the white circles represent the exhaust tubes. The dotted lines are approximate dimensions of the concrete sleeve lumped masses.

Figure 8 shows a face view of a section of the Hot TES with approximate virtual concrete sleeves. Note that in energy storage mode, all of the Hot TES mass was allocated to the working fluid tubes to derive the heat transfer coefficients and areas needed. In this new approach, U_{eff}^{*} and A_{eff}^{*} model the heat transfer between the steel tubing and the concrete. Further,

while Figure 8 shows missing mass on the edges of the dotted circles, in the model, all the concrete mass is evenly distributed across the working fluid tubes to derive $\mathrm{OR_{LM}}$.

Heat transfer from the fluid to the steel tubing was modeled through typical convective heat transfer using Gnielinski equations for turbulent flow in tubes [48], where the area term was the inner area of the steel tube ($A_{tube_{WF}}$). The energy balance system of equations was:

$$\rho_{\mathrm{tube_{WF}}} \mathrm{C}_{tube_{WF}} \mathrm{V}_{\mathrm{tube_{WF}}} \left(\frac{\partial \mathrm{T}_{\mathrm{tube_{WF}}}}{\partial \mathrm{t}}\right) = \mathrm{U}_{\mathrm{conv_{WF}}} A_{tube_{WF}} \left(\mathrm{T_{WF}} - \mathrm{T}_{\mathrm{tube_{WF}}}\right) + U^*_{eff} A^*_{eff} \left(\mathrm{T_{LM}} - \mathrm{T}_{\mathrm{tube_{WF}}}\right) \quad (2.7)$$

$$\rho_{\mathrm{LM}} \mathrm{C_{LM}} \mathrm{V}_{LM} \left(\frac{\partial \mathrm{T_{LM}}}{\partial \mathrm{t}}\right) = U^*_{eff} A^*_{eff} \left(\mathrm{T}_{\mathrm{tube_{WF}}} - \mathrm{T_{LM}}\right) \quad (2.8)$$

$$\dot{\mathrm{m}}_{WF} \left(\mathrm{h_{WF}}(\mathrm{z_{out}}) - \mathrm{h_{WF}}(\mathrm{z_{in}})\right) = U_{conv_{WF}} A_{tube_{WF}} \left(\mathrm{T}_{tube_{WF}} - \mathrm{T_{WF}}\right) \quad (2.9)$$

where the subscript WF stands for working fluid and LM stands for lumped mass.

The original model by Xu et al. was validated for energy storage mode. This new modified version was used for the Hot TES energy storage heat transfer; however, the Xu et al. modeling approach was not appropriate for the bottoming mode. Xu et al. derived the overall heat transfer coefficients assuming the outer boundary of the concrete cylinder had a zero temperature slope, i.e., at r=b, $\frac{\partial \mathrm{T_{LM}}}{\partial \mathrm{r}} = 0$. In bottoming mode, however, it was more appropriate to assume steady-state conduction across the concrete.

2.3.2.2. Bottoming Mode

While energy storage mode is inherently transient, the bottoming mode was best analyzed as a steady-state process. The steady-state heat transfer across a cylinder has a simple analytical solution:

$$R_{cyl} = \frac{\ln\left(\frac{OR}{IR}\right)}{2\pi L k} \quad (2.10)$$

where R_{cyl} is the thermal resistance across a cylindrical mass, OR is the outer radius of that cylinder, IR is the inner radius of that cylinder, L is the length of the cylinder, and k is the conductivity of the material [49].

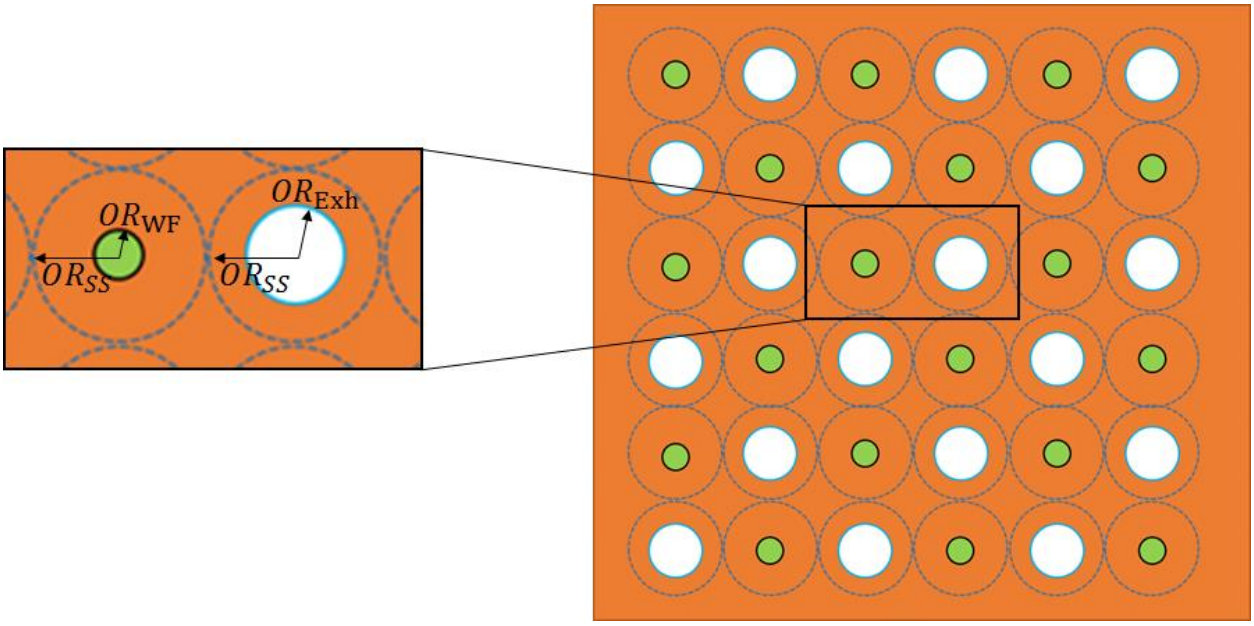

Figure 9: Visualization of lumped mass sleeves (face view) for heat transfer analysis in bottoming mode. The green circles represent the working fluid tubes, while the white circles represent the exhaust tubes. The dotted lines are approximate dimensions of the concrete sleeve lumped masses

Cylindrical symmetry was assumed for the heat transfer between the tubes in the solid state TES. This assumption was needed to derive the bottoming mode heat transfer coefficients. To do this, the same outer radius of the sleeve mass, $\mathrm{OR_{SS}}$, for both exhaust and working fluid tubes was used (Figure 9). In this case, the Hot TES mass was distributed to each tube type such that $\mathrm{OR_{SS}}$ was equal for both the working fluid and the exhaust tubes. This imposed a symmetry between the lumped masses, and allowed a point of intersection across the lumped mass. The thermal resistances became the resistance between $\mathrm{OR_{SS}}$ and the outer radius of each tube. The total lumped mass capacitance was then located at $\mathrm{OR_{SS}}$. Note that Figure 9 shows missing concrete mass at the edges of the dotted circles. In the actual model, the entire concrete mass was distributed to the working fluid and exhaust tubes to derive $\mathrm{OR_{SS}}$.

The energy balance system of equations for heat transfer to the lumped mass in bottoming mode was:

$$\rho_{\mathrm{tube_{WF}}} C_{\mathrm{tube}_{WF}} V_{\mathrm{tube_{WF}}} \left(\frac{\partial T_{\mathrm{tube_{WF}}}}{\partial t}\right) = U_{\mathrm{conv_{WF}}} A_{tube_{WF}} \left(T_{\mathrm{WF}} - T_{\mathrm{tube_{WF}}}\right) + \frac{2\pi L k_{LM}}{\ln\left(\frac{OR_{SS}}{OR_{\mathrm{WF}}}\right)} \left(T_{\mathrm{LM}} - T_{\mathrm{tube_{WF}}}\right) \quad (2.11)$$

$$\rho_{\mathrm{tube}_{Exh}} C_{\mathrm{tube}_{Exh}} V_{\mathrm{tube}_{Exh}} \left(\frac{\partial T_{\mathrm{tube}_{Exh}}}{\partial t}\right) = U_{\mathrm{conv_{Exh}}} A_{tube_{Exh}} \left(T_{Exh} - T_{\mathrm{tube}_{Exh}}\right) + \frac{2\pi L k_{LM}}{\ln\left(\frac{OR_{SS}}{OR_{\mathrm{Exh}}}\right)} \left(T_{\mathrm{LM}} - T_{\mathrm{tube_{Exh}}}\right) \quad (2.12)$$

$$\rho_{\mathrm{LM}} C_{\mathrm{LM}} V_{LM} \left(\frac{\partial T_{\mathrm{LM}}}{\partial t}\right) = \frac{2\pi L k_{LM}}{\ln\left(\frac{OR_{SS}}{OR_{\mathrm{WF}}}\right)} \left(T_{\mathrm{tube_{WF}}} - T_{\mathrm{LM}}\right) + \frac{2\pi L k_{LM}}{\ln\left(\frac{OR_{SS}}{OR_{\mathrm{Exh}}}\right)} \left(T_{\mathrm{tube_{Exh}}} - T_{\mathrm{LM}}\right) \quad (2.13)$$

$$\dot{m}_{WF} \left(h_{\mathrm{WF}}(z_{\mathrm{out}}) - h_{\mathrm{WF}}(z_{\mathrm{in}})\right) = U_{conv_{WF}} A_{tube_{WF}} \left(T_{tube_{WF}} - T_{\mathrm{WF}}\right) \quad (2.14)$$

$$\dot{m}_{Exh} \left(h_{\mathrm{Exh}}(z_{\mathrm{out}}) - h_{Exh}(z_{\mathrm{in}})\right) = U_{conv_{Exh}} A_{tube_{Exh}} \left(T_{tube_{Exh}} - T_{\mathrm{Exh}}\right) \quad (2.15)$$

where the subscript Exh stands for the exhaust fluid.

2.3.3. Compressors, Expanders, and Pumps

It is recognized that reciprocating machines have mass flows dependent on the volumetric displacement and the density of the fluid. The volumetric displacement is dependent on the pressure ratio and dead volume of the machine, as well as the speed at which the machine cycles. The speed and dead volume will affect the efficiency. The density of the fluid is dependent on the operating conditions, which are largely dependent on the evaporator/condenser performance, and the ambient temperature. Therefore, determining the mass flow involves many parameters.

To address this complexity, the proposed system model specified a mass flow *a priori* to create design requirements for the reciprocating machines. Machine isentropic, mechanical, and electrical efficiencies were used to calculate fluid states and energy flows across the machines. Since the goal of this work was to first understand the overall system behavior before performing detailed modeling for each component, this approach was favored to simplify the analysis of the system performance.

2.3.4. Cold TES

The Cold TES in the proposed system was an evaporator/condenser, which interacts with ambient air via a fan. To model the evaporator/condenser, an overall heat transfer coefficient was calculated by modeling a fan-forced convection in series with the resistance of the evaporator/condenser coils. This overall heat transfer coefficient was then used to calculate the heat transfer into or out of the fluid using a log mean temperature difference as:

$$\dot{\mathrm{Q}}_{\mathrm{cTES}} = \mathrm{U}_{\mathrm{cTES}}\mathrm{A}_{\mathrm{cTES}}\Delta\mathrm{T}_{\mathrm{Log}_{\mathrm{cTES}}} \tag{2.16}$$

where $\dot{\mathrm{Q}}_{\mathrm{cTES}}$ is the heat transfer, $\mathrm{U}_{\mathrm{cTES}}$ is the overall heat transfer coefficient, $\mathrm{A}_{\mathrm{cTES}}$ is the evaporator/condenser area, and $\Delta\mathrm{T}_{\mathrm{Log}_{\mathrm{cTES}}}$ is the log mean temperature difference [50].

To determine the overall heat transfer coefficient $\mathrm{U}_{\mathrm{cTES}}$, equations were based on the Cold TES design being considered [51]. The baseline design used an air-cooled plane tube heat exchanger. The model for that design used theory from Wang et al. 2006 [52].

Fans were used to enhance convection with the evaporator/condenser and were modeled as

$$\dot{\mathrm{W}}_{\mathrm{electric}_{\mathrm{fan}}} = \frac{\dot{V}_{fan}\Delta\mathrm{P}_{\mathrm{fan}}}{\eta_{\mathrm{fan}}} \tag{2.17}$$

where $\dot{\mathrm{W}}_{\mathrm{electric}_{\mathrm{fan}}}$ is the electric power of the fan, $\dot{V}_{fan}$ is the volumetric flow of air, $\Delta\mathrm{P}_{\mathrm{fan}}$ is the pressure rise across the fan, and η_{fan} is the fan efficiency.

2.3.5. TES Utilization

Another important model parameter is the level of TES charging and discharging, or TES utilization, φ, which in this study was defined as:

$$\varphi = \frac{E_{FCS} - E_{FDS}}{E_{ref}} \tag{2.18}$$

where E_{FCS} is the energy in the TES at the fully charged state, E_{FDS} is the energy of the TES at the discharged state, and E_{ref} is the energy required to raise the TES from ambient to the peak system temperature when fully charged.

2.3.6. Overall Efficiency Breakdowns

The overall energy storage round-trip efficiency was defined in section 1 as:

$$\eta_{ES} = \frac{W_{Tot}^{Dis}}{W_{Tot}^{Ch}} \tag{2.19}$$

where the charge and discharge work are:

$$W_{Tot}^{Ch} = \int_{t(E_{FDS})}^{t(E_{FCS})} \left[\dot{W}_{electric,CE}^{Ch} - \dot{W}_{electric,EC}^{Ch} + \dot{W}_{fan}^{Ch} \right] dt \tag{2.20}$$

$$W_{Tot}^{Dis} = \int_{t(E_{FCS})}^{t(E_{FDS})} \left[\dot{W}_{electric,CE}^{Dis} - \dot{W}_{electric,EC}^{Dis} - \dot{W}_{fan}^{Dis} \right] dt \tag{2.21}$$

In each case, $t(E_{FDS})$ is the time at the start of a fully discharged energy state (E_{FDS}), and $t(E_{FCS})$ is the time at the start of a fully charged energy state (E_{FCS}).

In addition to calculating the energy storage round-trip efficiency, the bottoming efficiency of the system was calculated as:

$$\eta_{Bot} = \frac{W_{Tot}^{Bot}}{Q_{Available}^{Bot}} \tag{2.22}$$

where the W_{Tot}^{Bot} is the same equation as the discharging case, but integrated over the bottoming period. $Q_{Available}^{Bot}$ is the heat available from the exhaust during bottoming.

In the next section, experimental results were used to validate the Hot TES model, as well as the new Simscape domain. The Cold TES and machinery models used standard methods and were checked against industry standard predictions/estimations, but they were not validated. Part B of this two-part paper presents the results of the model described here, including system analysis and key findings on PTES with waste heat harvesting.

2.4. Model Validation

While the machinery and evaporator/condenser models used conventional techniques, the Hot TES modeling approach was unique in this study. To validate the Hot TES model, two approaches were used.

First, a simple experiment was performed using a single straight tube cast in concrete. The purpose of this experiment was to validate both the modified Xu et al. model with the additional tube lumped mass, as well as the custom Simscape stead-state fluid domain developed here.

Second, a two-dimensional finite element analysis (FEA) was performed for the bottoming heat transfer mode, and compared to the lumped capacitance bottoming heat transfer model used in this study. The purpose of the FEA was to validate the simplified assumptions around the cylindrical geometry used in the bottoming heat transfer model.

2.4.1. Experimental Hot TES ES Validation

A small scale Hot TES test setup was created to gather data for validation of the Hot TES model and the custom Simscape steady-state fluid domain. The tests used air as the working fluid and involved multiple charge/discharge cycles.

The dimensions of the concrete block specimen tested were 0.10m x 0.10m x 2.0m. The block was cast around a 3/8 inch A179 carbon steel tube. A picture of the test specimen for the experimental setup is shown in Figure 10.

Table 2 lists the devices used for measurements in the test setup. A total of 40 type-K thermocouples were embedded within the concrete at 10 regular intervals along the length. Four thermocouples evenly distributed were placed in each interval arranged in a single line from the tube surface to the corner of the concrete block, as shown in Figure 10. The thermal properties were measured using a transient line heat source method (KD2 Pro by Decagon Devices); the values are shown in Table 3.

Measurement	Manufacturer	Sensor Name
Temperature	Omega	Type K Thermocouple
Pressure	Pro Sense	SPT25 Series Pressure Transmitters
Volumetric Flow	Preso	FT8-8AEBA-GEA-2 Flowmeter
Data Acquisition	Beckhoff	C6930-0040

Table 2: Measurement equipment used for experimental validation.

Thermal conductivity, k	1.32 W/m/K
Specific heat, Cp	725 J/kg/K
Density, ρ	2328 kg/m3

Table 3: Measured thermal properties of tested concrete block specimen

The test setup included a compressed air source, an electric air heater, a turbine flow meter, and a series of automated valves that switched the flow between charge and discharge modes. Temperature and pressure were measured before and after the block and before the flow meter. The concrete block was insulated with 8-inch panels of mineral wool.

Figure 10: Picture of the tube-in-concrete test specimen before being wrapped in insulation.

Data recording and controls were handled by a Beckhoff PLC controller connected to a personal computer. The Beckhoff unit controlled the valves to regulate flow speed, switched the heater on/off, and automatically switched between charge and discharge modes. Temperatures, pressures, and flow rate were recorded at 10 Hz. Temperature, flow, number of cycles, and cycle time were programmed for each test.

Temperature, pressure and flow data were processed using Matlab. Each signal was processed using a moving average filter with a window size of 10 points, then resampled down to 1 Hz. Calibration data was used to convert the flow meter frequency readings to volumetric flow then to mass flow (with fluid density determined from the temperature/pressure measurements). Flow enthalpy data were also determined (using REFPROP and CoolProp) at the pressure and temperature measured before and after the block. Processed flow property data and initial concrete temperatures were then compiled into a data object for use as input parameters into the model.

The model inputs generated from the experiment datasets included enthalpy and pressure of the air on the hot side and the cold side, mass flow rate, and the average initial temperature of the concrete at each section. During charge mode, when heated air flowed into

the hot side of the TES, the model used the hot side enthalpy, pressure, and mass flow experimental measurements as inputs to the model. The model then estimated concrete temperatures and cold side enthalpy. During discharge mode, when air at ambient temperature flowed into the cold side of the TES, the model used the cold side enthalpy, pressure, and mass flow experimental measurements as inputs to the model. The model then estimated concrete temperatures and hot side enthalpy. Concrete temperature states were retained between mode switches.

The difference between the model and experimental measurements were calculated for cold side air temperatures, hot side air temperatures, concrete section temperatures, and fluid enthalpy change between entrance and exit of the entire tube-in-concrete apparatus. The normalized root mean squared deviation between the simulation and experiment was calculated for each metric. The most important metric was considered to be the fluid enthalpy change, which leads to accurate energy transfers and fluid temperatures over time.

Uncertainty propagation was compiled from manufacturer error data for the sensors and data acquisition system. The fluid enthalpy change uncertainty for all validation experiments conducted in this study had an average upper bound of +7.2% and an average lower bound of -6.9%. These uncertainty values were due primarily to the pressure transmitters, which were used at about 30% of their maximum range.

Uncertainties in the experimental setup included actual material properties and heat losses through sensors, tubing fittings, and insulation on the test apparatus. These parameters were adjusted within expected ranges as part of the calibration of the model.

The drift in fluid energy between simulation and experiment for a typical case is shown in Figure 11. The upward trend is due to a net transfer of energy from the air to the concrete block over 4 charge and 4 discharge cycles. The average error in cumulative fluid energy between simulation and measurement was +/- 0.3% per hour, for a total of 13 experiments lasting between 10 and 12 hours each. This error was considered adequate for accurate implementation of the TES model and custom Simscape domain into the Bot-PTES model.

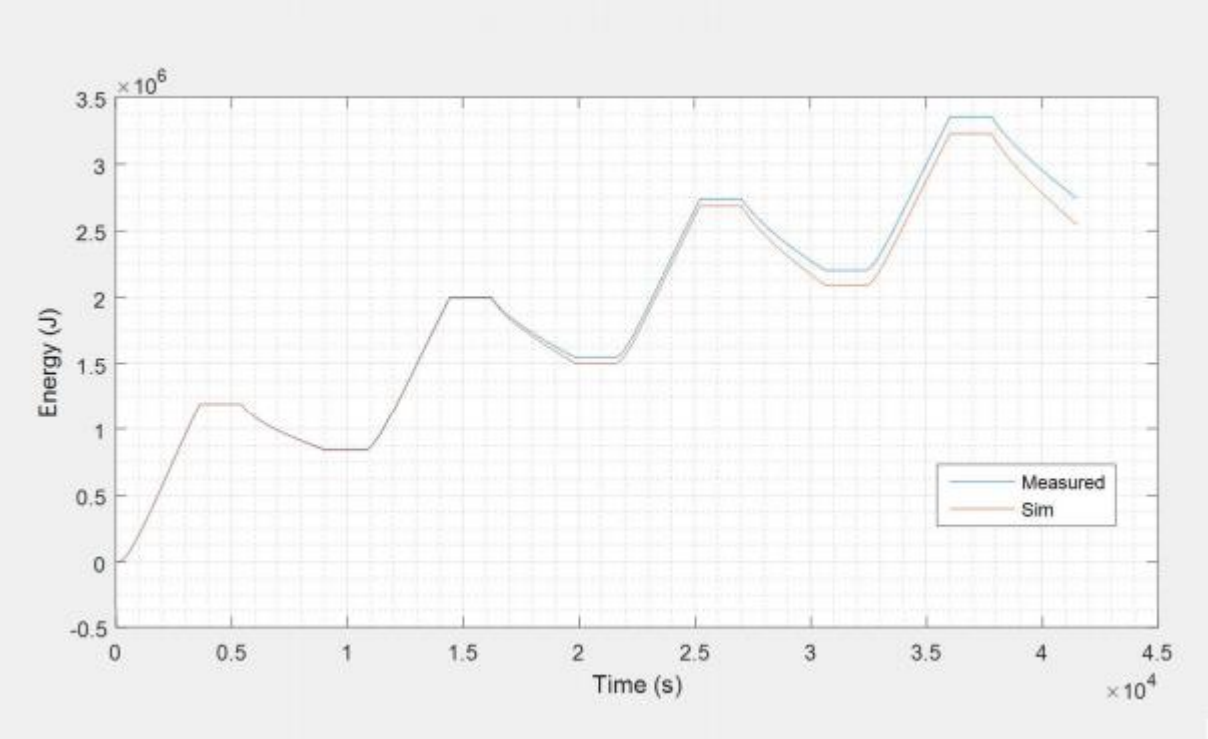

Figure 11: Measured and simulated cumulative energy leaving the fluid over time.

2.4.2. Heat Transfer FEA Hot TES Validation

The Hot TES bottoming mode 1D heat transfer model was validated using a two-dimensional Finite Element Analysis (FEA) model built using SolidWorks Simulation 2015 SP 5.0. The model analyzed the steady-state heat transfer between the exhaust tubes and the ammonia tubes.

Exhaust tube outer diameter	0.025 m
Exhaust tube wall thickness	0.001 m
Ammonia tube outer diameter	0.00925 m
Ammonia tube wall thickness	0.0017 m
Concrete face area	0.0035 m2
Concrete specific heat	970 J/kg/K
Concrete thermal conductivity	1.2 W/m/K
Concrete density	2400 kg/m3

Table 4: Geometry parameters used in the FEA model.

The geometry parameters chosen for this study are shown in Table 4. A simplified model geometry was created by taking advantage of symmetry in the TES block design (Figure 12). A

SolidWorks standard mesh was used to generate a target element size of 0.9622 m and tolerance of 0.04811 m. Bonded contacts were used at the concrete-tubing interfaces. The mesh model is shown in Figure 13.

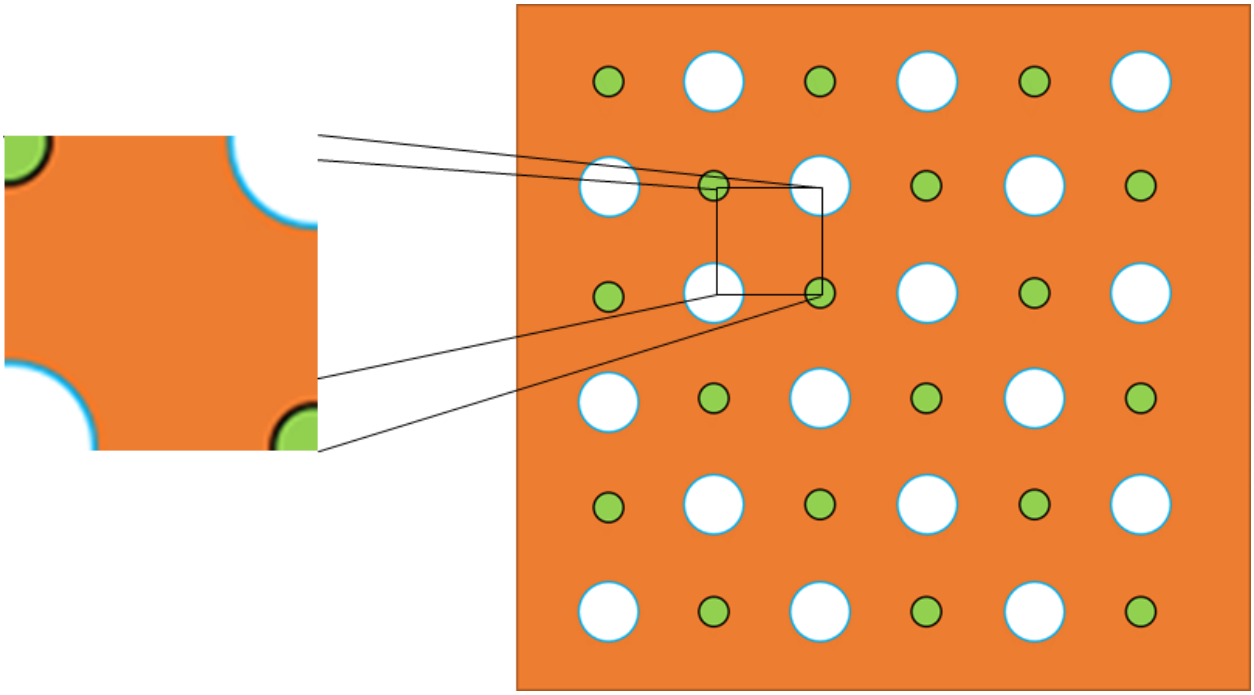

Figure 12: Symmetric simplification of a hot TES block.

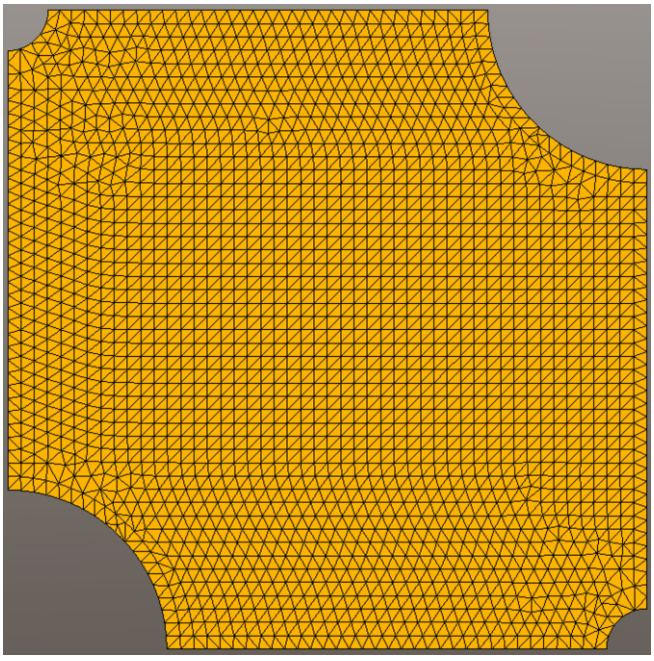

Figure 13: The mesh in the FEA model.

The load cases simulated by the thermal FEA are shown in Table 5. Constant temperature conditions were applied to the inside edges of each fluid tubing. Various combinations of temperature values for the ammonia and exhaust tubing were explored to determine model performance over a range of temperature differences (although temperature difference was not expected to affect the comparison). The initial temperature of the concrete block was not defined since this was a steady state analysis. After each simulation, concrete average temperature and average flux through the inside tubing edges were recorded.

Case #	NH3 Temperature [K]	Exhaust Temperature [K]
1	445	455
2	445	460
3	445	465
4	445	470
5	440	470
6	430	470

Table 5: FEA load cases.

For all cases analyzed, the Simscape model consistently under-predicted heat transfer by an average of 0.8%, and over-predicted the absolute temperature of the concrete mass by an average of 0.2%. Both percentage errors were relative to the FEA values. This systematic error between the Simscape and FEA models was deemed acceptable.

It was concluded that the 1D Simscape model under-predicted the bottoming mode heat transfer (over-predicted the thermal resistance) because the 1D model uses the entire concrete mass around the tubes to create its virtual cylinder dimensions. This effectively creates a longer heat transfer path length between the exhaust and ammonia tubes when compared to the actual 2D geometry.

2.5. Bot-PTES Concept and Model Conclusions

The challenge of designing a Bot-PTES system resides in its dual function—energy storage and bottoming. The two main design requirements for the Bot-PTES system were the requirement for net heat rejection for bottoming operation, and the ability to operate between

room temperature and natural gas turbine exhaust flow temperatures. The overall system design presented in this work meets these requirements while using positive displacement machines.

The model created for analyzing the proposed Bot-PTES system combined commonly used thermodynamic analysis methods along with unique components, which have been validated in this work. The model presented here was considered adequate for steady-state fluid flow system analysis in order to get estimated system efficiency and electric power values. Part B of this two-part paper shows results of a sensitivity analysis with the proposed model outlined in part A and presents a baseline design with its expected performance.

3. Chapter 3: Bot-PTES Sensitivity Analysis and Baseline Performance

This section of the dissertation uses the presented Bot-PTES model to evaluate key design parameters of the Bot-PTES system, it maps out its performances as stand-alone PTES and Bottoming systems, and it gives the expected performance in an example Bot-PTES application.

For this work, a Bot-PTES system was analyzed as an addition to a natural gas peaker plant. Natural gas peaker plants are designed to run only during hours of peak demand to add power capacity to the grid. They are typically installed as a single-cycle (no bottoming cycle) system. Connecting the Bot-PTES system to a natural gas peaker plant allows the Bot-PTES system to harvest heat leaving the peaker plant that would otherwise be wasted. The Bot-PTES could then be used as a utility-scale energy storage system for the hours of the day when the peaker plant is not running.

Figure 14 shows the proposed Bot-PTES system design. The states and properties are shown in the figure and are derived from the analysis of the baseline system presented here. These states depend on the operating conditions of the system, which are constantly in flux; therefore, these values are examples only.

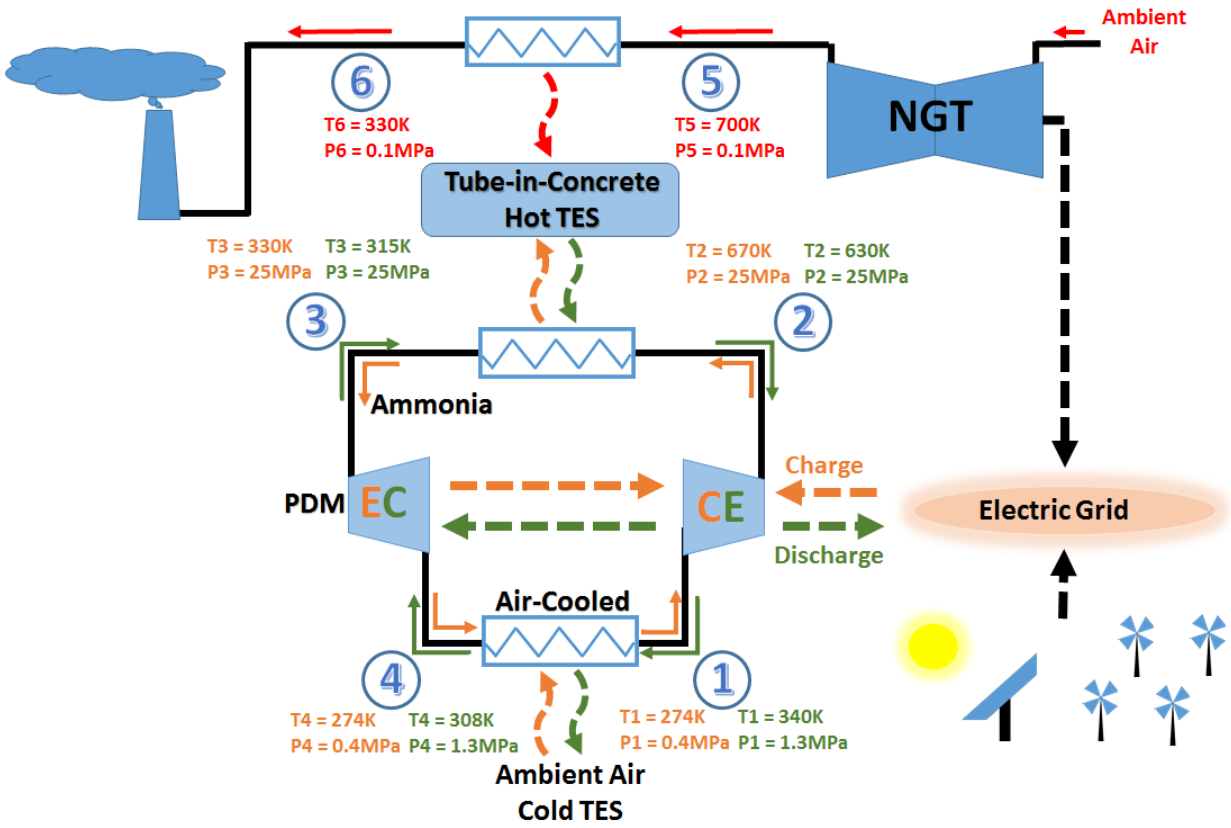

Figure 14: Bot-PTES system diagram where CE = Compressor/Expander, EC = Expander/Compressor, PDM = Positive Displacement Machine, NGT = Natural Gas Turbine (peaker plant). Energy flows are in dashed lines. Wavy lines represent heat flows. Solid lines represent fluid flows.

3.1. Analysis Methods

The time-domain model presented in Part A of this two-part report was run to iteratively determine the baseline design. All simulations used a constant 60-second time step. The baseline design was selected through a combination of requirements, feasibility, and optimal performance. Requirements of the system assumed *a priori* for this analysis were: a) 4 hours of storage at nominal discharge power, and b) matching the absorbed bottoming system heat power with the exhaust gas heat source power. The feasibility was mostly determined by reported literature.

For this study, three critical parameters were investigated in the design simulations: the Hot TES utilization, the evaporator/condenser size, and the peak system pressure. The results presented here show how the performance of this Bot-PTES system was affected by these

design parameters. Detailed design parameters such as the Hot TES concrete thickness and evaporator/condenser fins per inch were not investigated in this study.

The state of the exhaust leaving the natural gas turbine peaker plant (Figure 14) was specified by mass flow and assumed temperature and pressure. A temperature of 700K was selected for this state, because the Bot-PTES working fluid (ammonia) states were only available up to 700K in the simulation database used in this study (NIST REFPROP version 9.1 and/or CoolProp version 5.1.2). Most natural gas turbine exhausts are above 700K [53][54]; therefore, using 700K was a conservative value for characterizing the expected Bot-PTES performance. Higher temperatures should yield better efficiencies.

3.1.1. Stand-Alone Energy Storage Operation

First, the Bot-PTES system was analyzed as an energy storage (ES) system in isolation (i.e., no bottoming operation). The nominal operating ES mode assumed a constant mass flow of ammonia during both charge and discharge. Hot TES profiles are known to drift over consecutive charge/discharge cycles when initializing from a random temperature state of the Hot TES [17]. Therefore, to determine long-term behavior of the model, the system was fully charged/discharged 9 times before the system performance was calculated. The performance metrics were evaluated after the 10th charge/discharge cycle. The number of cycles was previously established to ensure convergence (less than 2% drift in energy state) of the Hot TES temperature gradients.

For this evaluation, an initial fully charged energy state and a specific Hot TES utilization level were selected. The Hot TES fully discharged state was specified as follows:

$$\mathrm{E_{FDS}} = \mathrm{E_{FCS}} - \varphi * \mathrm{E_{ref}} \tag{3.1}$$

where the Hot TES energy in the fully charged and discharged states are $\mathrm{E_{FCS}}$ and $\mathrm{E_{FDS}}$, respectively, and φ is the Hot TES utilization. In all simulations in this study, $\mathrm{E_{ref}}$ represents the maximum storage capacity, and was calculated using assumed minimum and maximum uniform temperatures of 288K and 685K, respectively. The Hot TES utilization was a parameter investigated in this study, while the fully charged state was optimized by maximizing the

efficiency for each design case. The approach for that optimization routine will be discussed below.

3.1.2. Stand-Alone Bottoming Operation

The Bot-PTES system was also evaluated as a stand-alone bottoming system in isolation (i.e., no ES operation). In the bottoming mode, exhaust from a natural gas plant flowed through the Hot TES. Simultaneously, the Bot-PTES system discharged the Hot TES to generate electricity. The Hot TES temperature gradients must also converge in bottoming mode. Convergence of the model in bottoming operation was unique to a system with a Hot TES between the two fluids exchanging heat. Having an ES capacitance between the exhaust heat source and the ammonia heat sink created a delay (while the temperature gradients formed) before reaching steady-state operation. For example, since there was heat available in the Hot TES regardless of the exhaust heat power, the ammonia could be pulling more heat from the Hot TES than the exhaust was injecting. Calculating the instantaneous electric power out of the ammonia system over the heat available from the exhaust under these conditions would over-predict bottoming efficiency. Consequently, to represent long-term steady operation, the simulation was run until an energy balance was met between the exhaust heat entering the Hot TES and the ammonia heat leaving the Hot TES, as determined by <0.1%/hr change in TES temperature gradients.

3.1.3. Energy Storage + Bottoming Operation

The Bot-PTES system was also evaluated as a combined system, cycling between bottoming and ES modes. For this case, the system was first brought to a fully charged state using grid electricity and no exhaust flow. During this charge period, the system ran at 40% of nominal mass flow. It was then operated in bottoming mode for four hours where the exhaust heated the Hot TES while the Bot-PTES system cooled (discharged) the Hot TES. During this bottoming period, the Bot-PTES system ran at nominal mass flow. Lastly, the system was brought to a fully discharged state without the exhaust flow running. During this ES discharge period, the Bot-PTES system ran at 67% of nominal mass flow for the working fluid. These

operating conditions were selected to represent the context of solar energy available to charge the system electrically during the day, with peaker plant heat available in the evening.

3.1.4. Coupled ES + Bottoming Efficiency Definitions

New efficiency definitions were created for viewing the coupled operation results. These new definitions helped compare the Bot-PTES system to other stand-alone ES systems. They also revealed differences in Bot-PTES system performance between stand-alone operation and coupled operation.

For this study, gross ES efficiency was defined as:

$$\eta_{\mathrm{ES,gross}} = \frac{\mathrm{W}^{\mathrm{Dis}}_{\mathrm{electric,net}}}{\mathrm{W}^{\mathrm{Ch}}_{\mathrm{electric,net}}} \tag{3.2}$$

where $\mathrm{W}^{\mathrm{Ch}}_{\mathrm{electric,net}}$ and $\mathrm{W}^{\mathrm{Dis}}_{\mathrm{electric,net}}$ were the integrated charge and discharge electric energies, respectively. The gross ES efficiency was used for comparisons to other ES solutions. In this study, the free heat energy was allocated to the ES in the efficiency calculation, and this step was intended to highlight the synergy that was being investigated. The peaker plant was rejecting that heat independently of whether an ES system was connected to it or not. The key advantage of PTES is that it utilizes this waste heat with the same equipment that it uses for its ES functions.

Lastly, effective ES efficiency was defined as:

$$\eta_{\mathrm{ES,effective}} = \frac{\mathrm{W}^{\mathrm{Dis}}_{\mathrm{electric,net}} - \eta^{*}_{Bot}\mathrm{Q}_{\mathrm{waste}}}{\mathrm{W}^{\mathrm{Ch}}_{\mathrm{electric,net}}} \tag{3.3}$$

where η^{*}_{Bot} is an assumed bottoming efficiency during coupled operation (taken from the stand-alone bottoming results). Here, the effective ES efficiency was determined by subtracting the electrical work generated by the waste heat input with an assumed bottoming efficiency. This term was defined in order to determine how the coupled Bot-PTES operation performance compared to the stand-alone operation.

3.1.5. Sensitivity Analysis

A sensitivity analysis of the system design parameters was performed and is illustrated in Figure 15. Each parameter was individually analyzed in reference to a baseline design, while all other parameters were held constant. This process was iterative, and some components of the baseline design were determined through the sensitivity analysis. The results presented here are the product of multiple iterations that led to the final baseline system design.

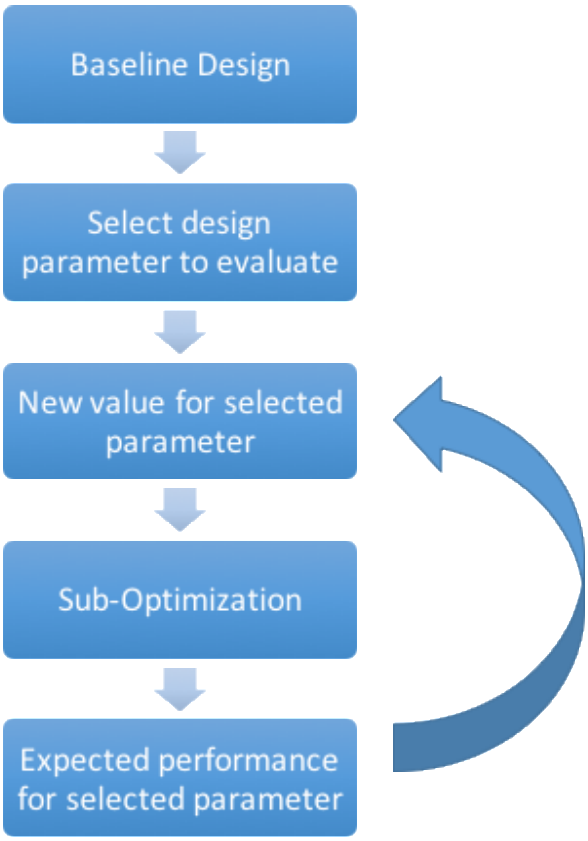

Figure 15: Sensitivity analysis procedure.

3.1.6. Sub-Optimizations

Sub-optimization routines to maximize efficiency were performed for each design parameter using the Mathworks 2016a Global Optimization Toolbox with the Pattern Search solver. Default settings were used for the solver. The sub-optimizations routines determined three key operational parameters: charge fan power, discharge fan power, and full charge state. The fan power was not optimized at every point in time during the simulation to limit

computation cost; however, it is recognized that the fan power changed during charge and discharge. Instead, near optimization was achieved through appropriate selection of constant fan power over the charge and discharge, separately.

A full simulation of the Bot-PTES for each operational parameter set was performed. After a simulation, the efficiency for that case was compared to previous iterations using the optimization algorithm. This process continued until the operational conditions were optimized to the default pattern search algorithm tolerances.

3.1.7. Baseline ES Efficiency Maps

A new performance metric called instantaneous round-trip efficiency was defined in order to generate ES efficiency maps for the baseline system:

$$\eta_{\mathrm{ES,instant}} = COP^{Ch} * \eta_{TE}^{Dis} \tag{3.4}$$

where COP^{Ch} is the coefficient of performance during charge, and η_{TE}^{Dis} is the thermal engine efficiency during discharge. This metric was used to estimate the ES efficiency that could be achieved if the system was to oscillate between charge and discharge an infinitesimal amount at a given state of charge. This procedure was used to identify where the best trade-off of COP and thermal engine efficiency was throughout the various charge states in the Hot TES.

To develop ES efficiency maps of the baseline system, the power was varied by varying the Bot-PTES mass flow from 20% to 100% of nominal, at 20% increments. The charge states were extracted from the simulation data every 60 seconds over the charge/discharge processes.

3.1.8. Levelized Cost of Energy

Energy generation technologies can be compared using a levelized cost of energy (LCOE) [32,55], which incorporates expected cash flows due to capital expenditures, debt payments, target rate of return, depreciation, taxes, operations and maintenance, and price escalation. LCOE was used in this study to compare the proposed Bot-PTES system to other ES systems and other common forms of energy generation.

The National Energy Technology Laboratory (NETL) created a simplified LCOE model, which integrates cash flow considerations into simple cost coefficients for any energy system [56]. In order to incorporate the additional cost required to charge an ES system, a modified version of the NETL LCOE calculation was developed:

$$LCOE_P = \frac{\left((CCF_P)(TPC)+\sum(LF_{Fn})(OC_{Fn})+(CF)\sum(LF_{Vn})(OC_{Vn})\right)}{(CF)(MWh)} + \frac{LCOE_{Ch}}{\eta_{\mathrm{ES,gross}}} \quad (3.5)$$

where $LCOE_P$ is the levelized cost of electricity over P years of the delivered energy from an ES system. CCF_P is the capital charge factor for a levelization period of P years, TPC is the capital cost, LF_{Fn} is the levelization factor for category n fixed operating cost, OC_{Fn} is the category n fixed operating cost for the initial year of operation, CF is the plant capacity factor, LF_{Vn} is the levelization factor for category n variable operating cost, OC_{Vn} is the category n variable operating cost at 100% capacity factor for the initial year of operation, MWh is the annual net MWh of power that would be generated at 100% capacity factor, and $LCOE_{Ch}$ is the levelized cost of energy required to charge the ES system. The simplified LCOE factors were extracted from an NETL report [32], and are shown in Table 6.

Lazard Ltd annually submits LCOE estimates for several energy sources ranging from conventional coal to photovoltaics. Values from the November 2015 report were used in the analysis presented here for $LCOE_{ch}$ estimates [55]. The report was also used to obtain the LCOE of conventional energy generation technologies used for comparison.

Parameter	Value
Income Tax Rate	38% Effective (24% Federal, 6% State less 1% property and 1% Insurance)
Repayment Term of Debt	15 years
Grace Period on Debt Repayment	0 years
Debt Reserve Fund	None
Depreciation	20 years, 150% declining balance
Working Capital	Zero for all parameters
Plant Economic Life	30 years
LCOE Levelization Period	20 years
Investment Tax Credit	0%
Tax Holiday	0 years
Start-Up Costs (% of EPC)	2%
All other additional capital costs ($)	0
EPC escalation	0%
Duration of Construction	3 years
Debt (% of total capital)	50%
Equity (% of total capital)	50%
Debt Interest Rate	9%
Equity Internal Rate of Return	12%
Capital Charge Factor	0.164
All Levelization Factors	0.1618

Table 6: Parameters used for LCOE calculations.

3.2. Baseline Bot-PTES Design Performance

3.2.1. Baseline System Inputs

Table 7 shows the baseline inputs for the system model. In this table, “machine” signifies all machinery in the system (i.e. compressors and expanders). The machine efficiencies were obtained from published literature on PTES reciprocating compressors/expanders [18,57]. The high pressure limit was based on published values of supercritical steam plant pressures currently available [53].

The proposed Hot TES design used concrete properties previously used by DLR [58], and dimensions deemed fabricable based on work at Bright Energy Storage Technologies LLP. For all design cases, the Hot TES was sized to obtain approximately 4 hours of storage when discharged at nominal power. The Hot TES was scaled by varying the number of concrete blocks

in parallel, where each concrete block contains one ammonia tube and one exhaust tube. The design also ensured minimal pressure peak drop across the Hot TES (< 0.05 bar for exhaust and < 1 bar for ammonia). A utilization factor of 20% was selected based on the results shown in the utilization sensitivity section below.

Ambient Temperature	288 K
Ambient Pressure	1.01325 bar
Machine Isentropic Efficiencies	99%
Machine Mechanical Efficiencies	92%
Motor/Generator Efficiencies	97%
Nominal Ammonia Mass Flow	18.5 kg/s
Nominal High Pressure	25 MPa
Hot TES Concrete Conductivity	1.2 W/m/K
Hot TES Concrete Specific Heat	970 J/kg/K
Hot TES Concrete Density	2400 kg/m^3
Length of Hot TES	100 m
Number of Ammonia Tubes in Hot TES	7000
Total Hot TES Concrete Volume	2450 m^3
Ammonia Hot TES Tube OD	9.53 mm
Ammonia Hot TES Tube Wall Thickness	1.65 mm
Exhaust Hot TES Tube OD	50.8 mm
Exhaust Hot TES Tube Wall Thickness	1 mm
Hot TES Utilization Factor	20%
Cold TES Design	Air-cooled heat exchanger, plain-finned, 8 fins-per-inch, 4 rows
Cold TES Area	100,000m^2
Exhaust Mass Flow	95 kg/s (Dry Air)
Exhaust Incoming Temperature	700K

Table 7: Key System Model Inputs.

The Cold TES used an air-cooled, plain-finned heat exchanger [51]. For this proposed system, a 100,000 m^2 evaporator/condenser was selected. It was sized for a 20-25 K difference between ambient air and ammonia condensation temperature during nominal bottoming discharge. This requirement made the system comparable to steam condenser temperature

differences shown in studies by NETL [53]. It was assumed that this temperature difference was optimized for cost and performance for the steam bottoming system. It was also assumed that a similar cost/benefit result would apply to an ammonia system.

3.2.2. Baseline Nominal Power Operation

ES Round Trip Efficiency	52.3%
Bottoming Efficiency	24.0%
Avg ES Charge Power [MW]	16.7
Avg ES Discharge Power [MW]	8.6
Avg Bottoming Discharge Power [MW]	9.7
Charge Time at Nominal Power [hours]	3.95
Discharge Time at Nominal Power [hours]	4

Table 8: Performance outputs of baseline system model under nominal conditions.

Table 8 shows the stand-alone ES and bottoming performances of the baseline system under nominal conditions. The ES efficiency of this proposed system (52.3%) was lower than those from other published PTES designs (typically over 60%). This reduced ES efficiency was mostly due to the high temperature difference of the air-cooled evaporator/condenser, and the evaporator/condenser fan power draw.

Results showed high electric charge power consumed during nominal operation. In an optimized system, this charge power should be lowered for several reasons. First, a large charge power requires increasing the capacity for all the electronics, which will increase cost. Second, it is likely that the system would be designed to displace a target power level on the grid (whether charge or discharge) and not an arbitrary value. For example, if it were connected to a photovoltaic (PV) plant and able to charge 10 MW of the PV capacity, it should be able to replace (discharge) that 10 MW of PV capacity when needed.

Nominal operation included a constant mass flow of 18.5 kg/s in both charge and discharge. This value was specified to simplify the analysis; however, in a real case, the reciprocating machines would operate with lower mass flow during charge mode due to lower density of ammonia during evaporation compared to condensation. For example, with a 30 K

temperature difference between evaporation in charge and condensation in discharge (State 4 in Figure 14), the density would be about 2-3 times lower in charge than in discharge mode.

Thus, during charge mode, the reciprocating CE device, operating as a compressor, would receive lower density ammonia from the evaporator than the same device, acting as a vapor expander, would eject to the condenser in discharge. If a single machine could function as the CE for both charge (compression) and discharge (expansion), then the CE could run at 2-3 times the speed in charge mode to keep the mass flow constant. This process would create higher pressure-drops across the valves and decrease efficiency. If a separate compressor and expander were used as the CE, then the compressor would have 2-3 times the volumetric flow as the expander, costing more capital. Instead, it is recommended that the system run at lower power (mass flows) but longer charge times.

Table 8 also shows that the Bot-PTES system produced a low heating value (LHV) bottoming efficiency of 24.0%. This value is lower than conventional steam bottoming cycles currently available. In a 2015 NETL report where 876 K exhaust entering a steam bottoming cycle was assumed, the steam system obtained approximately 39.1% efficiency at converting *absorbed* heat into *expander* electricity [53].

To better compare the NETL results to the Bot-PTES system presented here, both efficiencies were converted into a LHV efficiency at converting *available* heat to *net expander* electricity (expander electricity minus compression work from State 4 to State 3, Figure 14). With this new metric, the steam system obtained 32.2% LHV efficiency at converting available heat into net expander electricity, while the Bot-PTES system obtained 24.7% efficiency. Therefore, the Bot-PTES system was about 76.6% as efficient as the steam bottoming system analyzed in the NETL paper.

This comparison is somewhat unequal, since the steam system from the NETL paper used 876K exhaust, while the Bot-PTES system had only 700 K exhaust. As a reference, the Carnot efficiency limit increases by 8.3% going from 700 K to 876 K with 288 K ambient temperature. With the baseline Bot-PTES design, the net expander power was getting 42.0% of the Carnot limit. Assuming the Bot-PTES system still achieves 42.0% of Carnot at 876 K brings the bottoming efficiency up to 28.2%.

Ammonia is not as efficient as steam at creating work at high temperatures for several reasons. For any bottoming system, the low-pressure state (State 1, Figure 14) limits how much the CE can expand from a given high pressure to generate work. State 1 is fixed by the fluid condensation pressure. For example, expanding ammonia isentropically from 700 K down to saturated vapor at 305 K (1.2 MPa) requires a pressure of 57 MPa. At the maximum of 25 MPa for this system design, the CE can only expand isentropically down to about 356K, leaving 51 K of superheat which is not utilized for work. Furthermore, at pressures above 25 MPa, ammonia becomes highly incompressible (~< 0.03 %volume/MPa), requiring higher EC work compared to the CE work generated.

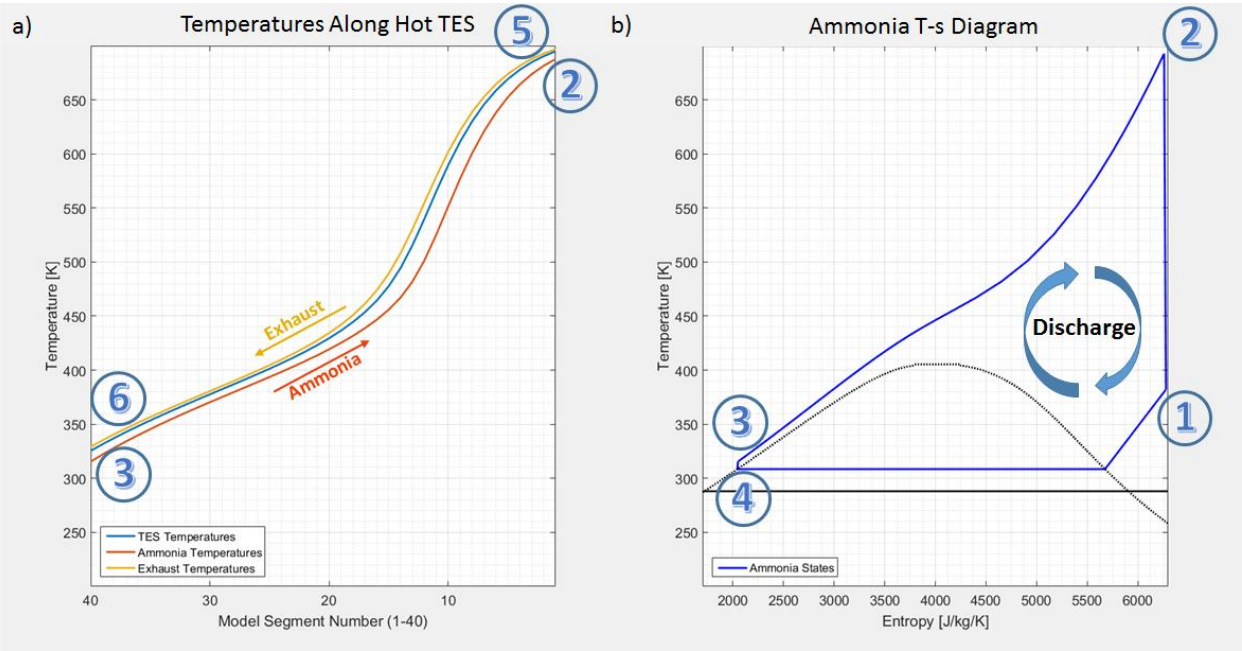

Figure 16: a) Temperature along the length of the Hot TES, and b) T-s diagram of ammonia for the baseline Bot-PTES design during nominal bottoming operation. Fluid states are labeled from 1 to 4.

One advantage of using ammonia with the Bot-PTES system is that the specific heat is fairly constant across all Hot TES temperatures at the supercritical high pressure of the system. Additionally, the large heat transfer area required for the ES operation lowers the temperature differences on the hot end. Both of these attributes improve the temperature difference between ammonia and exhaust when compared to conventional steam bottoming. As a

comparison, the proposed Bot-PTES system captured about 90% of the heat available at 700 K, while the steam bottoming system presented by NETL achieves about 84% capture at 876 K.

3.2.3. Baseline ES Performance Maps

In energy storage mode without bottoming, the baseline Bot-PTES design showed a range of performance depending on power levels and Hot TES charge states as illustrated in Figure 17 to Figure 20. Figure 17 shows the overall (round-trip) efficiency as a function of power level. For all cases considered, a 20% utilization was assumed for the Hot TES in both charge/discharge modes. The efficiency increased with the lower power levels. The lower power levels were achieved by lowering the system mass flow. This in turn lowered heat exchanger temperature differences throughout the system and steepened the Hot TES temperature gradients, both of which improved the round-trip efficiency.

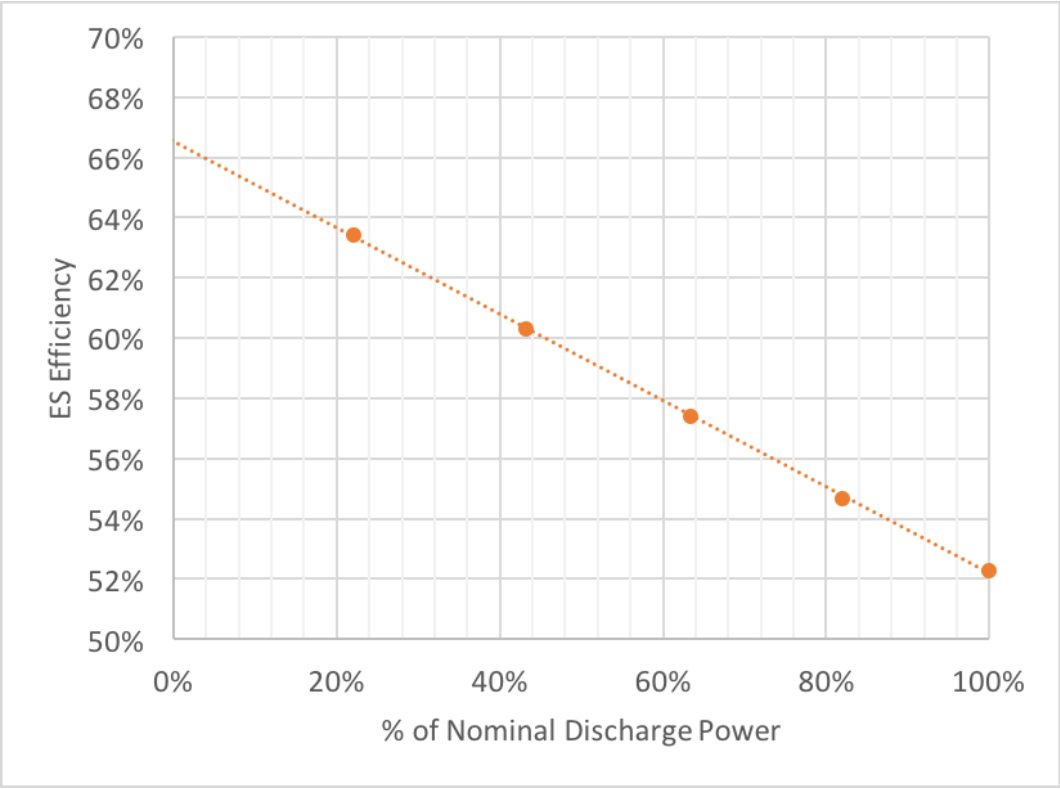

Figure 17: Effect of discharge power on round-trip ES efficiency.

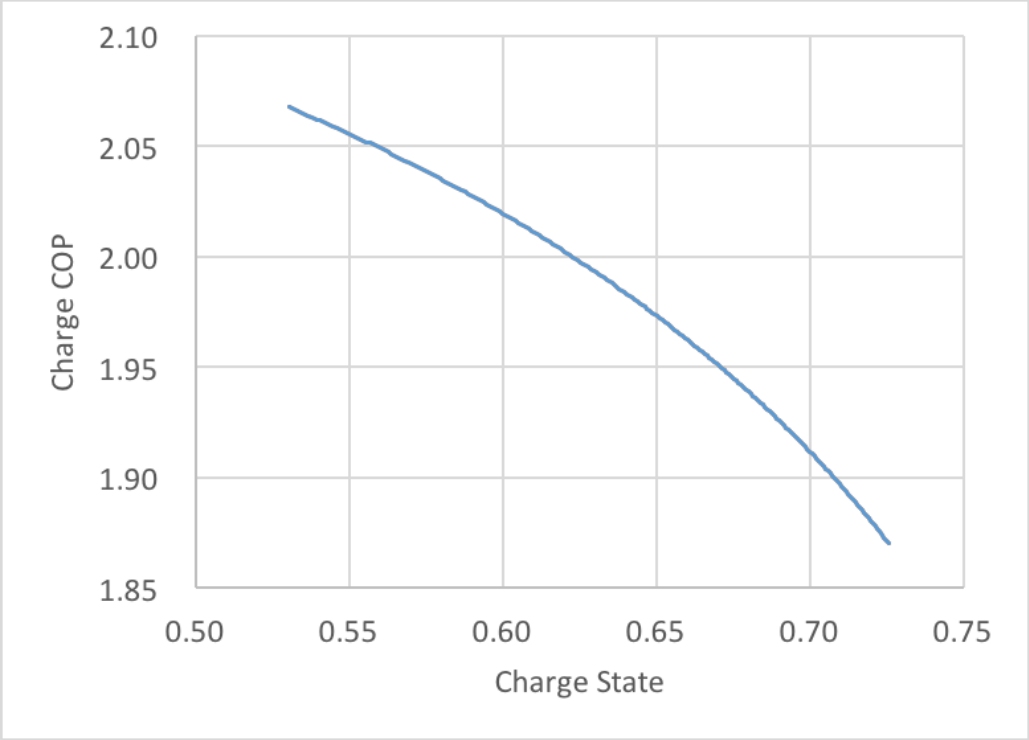

Figure 18: Effect of charge state on nominal power charge COP.

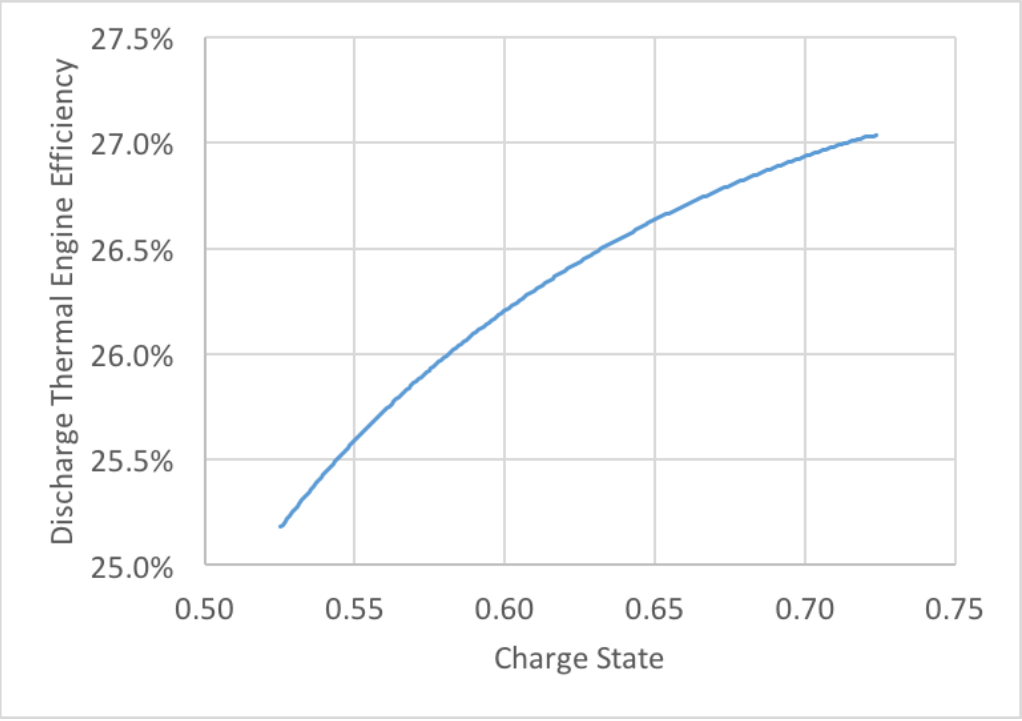

Figure 19: Effect of charge state on nominal power discharge thermal engine efficiency.

Figure 18 shows how COP^{Ch} varies with charge state. Note that as the charge state increases, the COP drops because the Hot TES captures less and less heat relative to the overall energy input for the system. Figure 19 shows η_{TE}^{Dis} as a function of the level of nominal discharge power. Note that η_{TE}^{Dis} decreases more (i.e., steeper slope) at lower charge states, as the temperature leaving the Hot TES decreases. These conflicting trends result in an optimum instantaneous round-trip efficiency, as shown in Figure 20. Peak efficiencies occur at around a charge of 0.60 for all power levels considered in this study (22 to 100%). The highest efficiency determined was 65.2%, which occurred at a nominal power of 22%, near a charge state of 0.57.

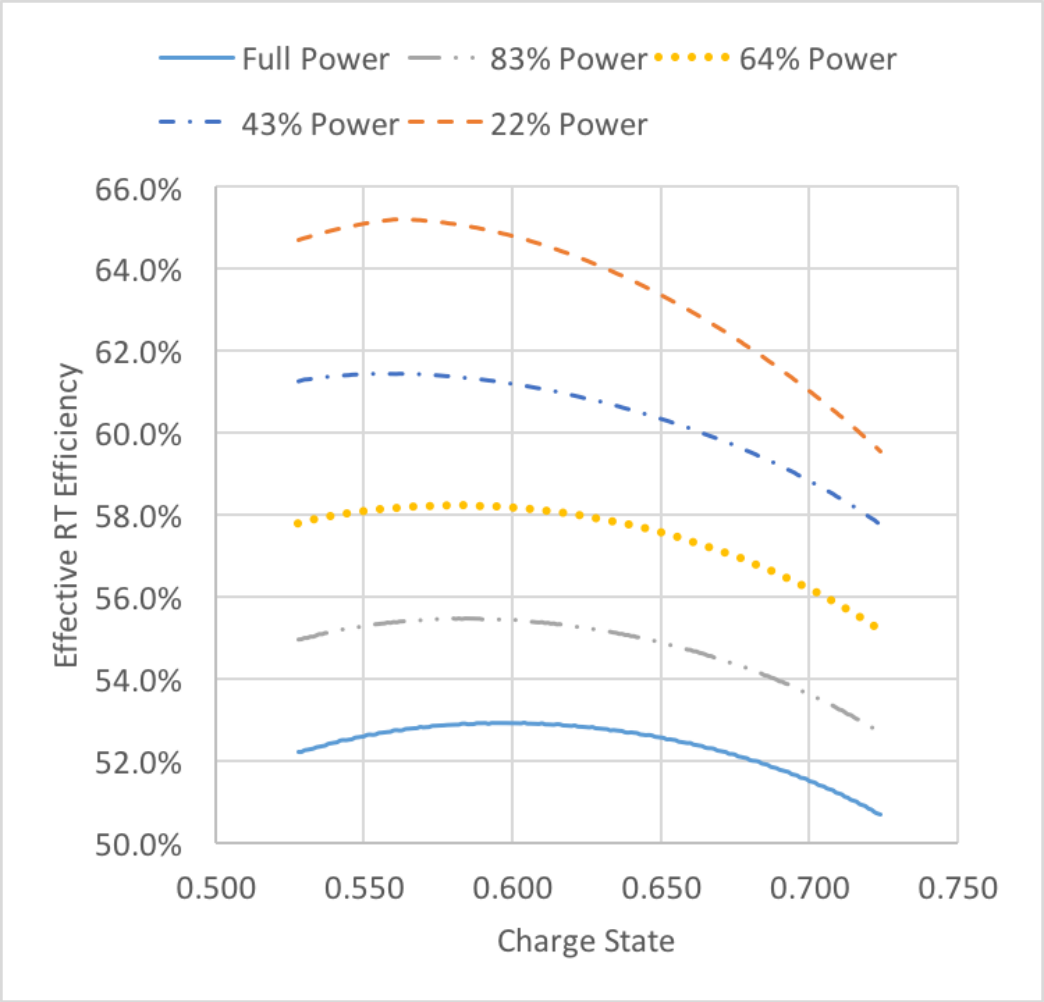

Figure 20: Effects of both charge state and power level on effective ES efficiency.

Results showed that with decreased power the instantaneous round-trip efficiency became more sensitive to variations in charge state. At lower power levels, the Hot TES temperature gradients increased, keeping the temperature lower on the cold end of the Hot TES for more of the charge process. However, as the temperatures increased on the cold end later in the charge process, they rose faster per increase in charge state due to these steeper gradients, resulting in the observed increase in sensitivity of efficiency to charge state.

3.3. Sensitivity Results

3.3.1. Hot TES Utilization

Hot TES utilization is defined as the percent of Hot TES capacity that is utilized for the energy (heat) storage operation. If 100% of the Hot TES is utilized, the entire block becomes saturated at the maximum temperature of operation in the fully charged state, and then completely cools to ambient temperature in the fully discharged state. The more a Hot TES is utilized, the lower capital cost needed for the same storage capacity. However, the more a Hot TES is utilized, the more the efficiency will decrease due to incomplete cooling of the WF in charge mode or incomplete heating in discharge. Consequently, optimization of this system requires careful consideration of capital vs operating cost tradeoffs.

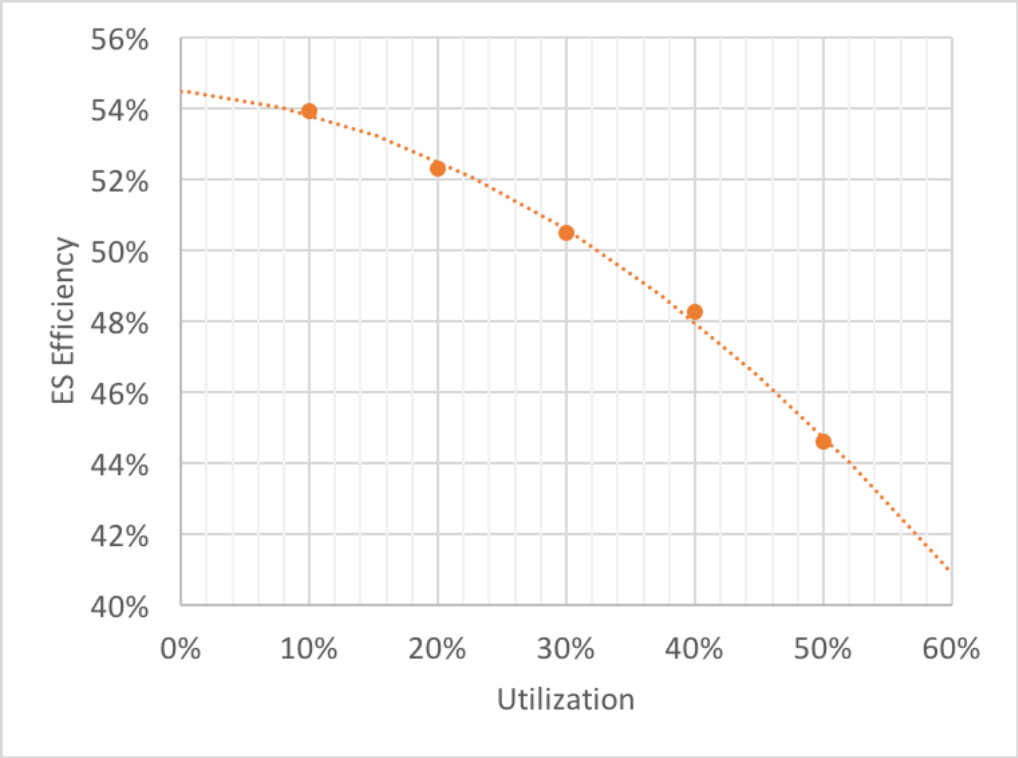

Figure 21: Effect of Hot TES utilization on RT ES efficiency.

Figure 21 gives the ES round-trip (RT) efficiency for utilization levels varying from 10% to 50%. A quadratic function was fit to the data, revealing the nonlinear penalty on efficiency with increasing utilization. Figure 22 is not-to-scale graphic to demonstrate the effects of the Hot TES temperature gradients. The arrows represent the direction of flow during charge and discharge. As the fully charged state increases (higher utilization), the cold side temperature increases, leading to decreasing capture of heat by the Hot TES and decreasing efficiency. Similarly, as the fully discharged state decreases (higher utilization), the hot side temperature of the Hot TES decreases, reducing the work out through the CE during expansion, and reducing the overall efficiency. These effects lead to the quadratic decline in efficiency with increasing utilization.

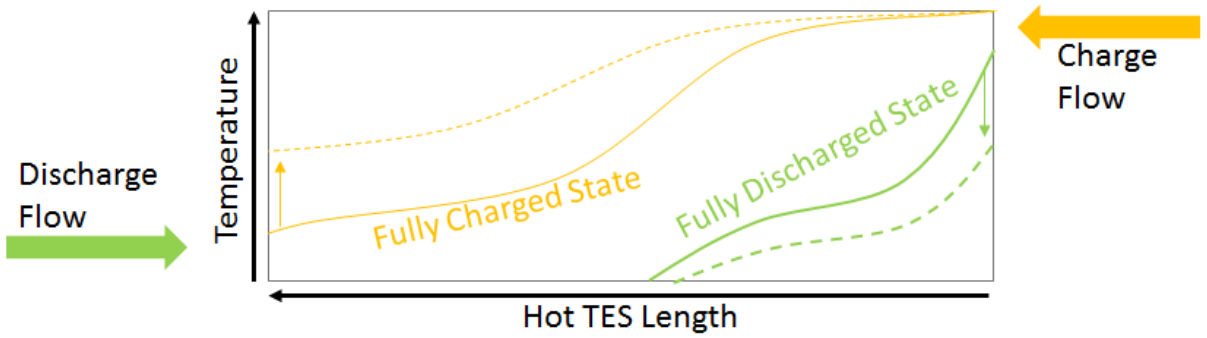

Figure 22: Not-to-scale representation of temperate gradients across the Hot TES length. Solid lines represent fully charged and discharged states for low utilization; dashed lines represent charged states for high utilization.

This study also investigated how utilization affects the liquid expander/compressor (EC) design. Figure 23 shows the EC operating points near the end of the charge mode for varying Hot TES utilizations. The red lines show an isentropic expansion from the fluid state leaving the Hot TES (State 3, Figure 14), down to the LP point (State 4, Figure 14). During nominal operation, the EC expands the relatively low temperature, high-density supercritical ammonia down to a low pressure, mostly liquid state. As the utilization increases, the liquid expander must handle higher fluid temperatures and qualities. This process ultimately leads to a wider range of fluid densities, which the EC must manage throughout the charge and discharge operation.

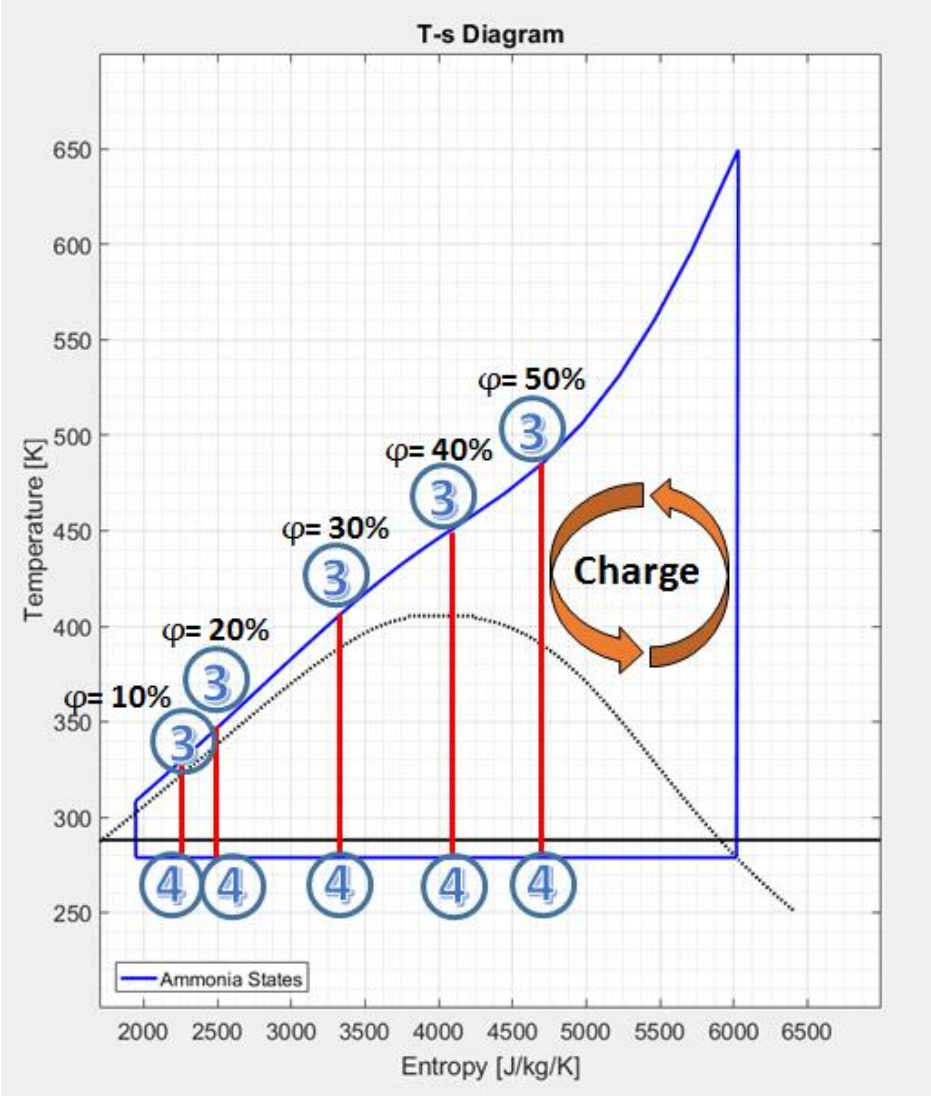

Figure 23: Liquid expander temperature ranges during charge mode for varying utilization. The red lines show isentropic expansion points at the end of charge mode for the EC (State 3 to State 4).

For the proposed baseline Bot-PTES system, the selected nominal Hot TES utilization was 20%. This value limited the design challenges of the EC, like the range of fluid densities, while maximizing utilization and increasing system efficiency. Optimization of the Hot TES utilization for this system will require an in-depth analysis of the ammonia EC as well as system cost-performance trade-offs

3.3.2. Evaporator/Condenser Size

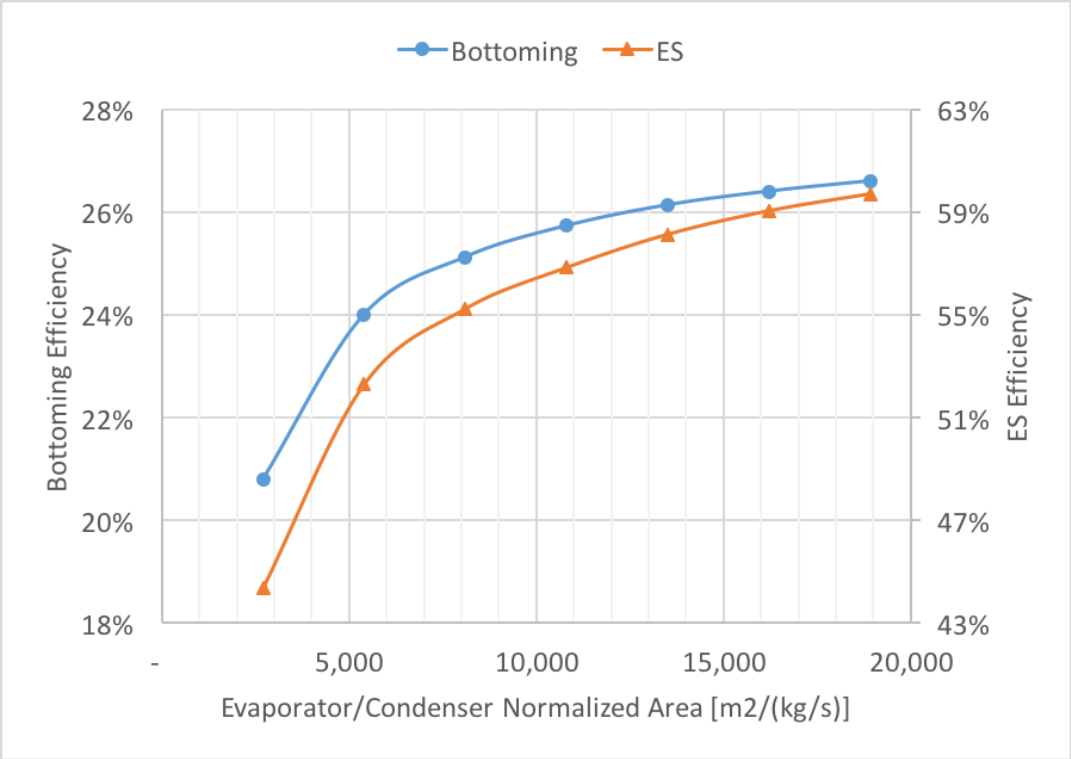

Figure 24: Evaporator/condenser area performance sensitivity.

The evaporator/condenser acting as the Cold TES was found to significantly affect the performance of the Bot-PTES system. Figure 24 shows how the size of the air-cooled evaporator/condenser affects both the bottoming and ES efficiencies. The area was normalized by the ammonia flow rate. Note that the area of the evaporator/condenser has limited impact on improving the system efficiencies. This is due to the inverse relationship between the evaporator/condenser area and the evaporation/condensation ΔTcold—the temperature difference between ambient temperature and the ammonia evaporation/condensation—and the system efficiencies are linearly dependent on ΔTcold (Figure 25).

Figure 25 shows how the system efficiency declines linearly with ΔTcold during discharge (condensation). The performance without the evaporator/condenser fan is included in Figure 25 to show the impact the fan power has on the system efficiencies. The lines represent linear fits through the data points, which extrapolate the results. The data points in Figure 25 correspond to those in Figure 24. Figure 25 was included to help decouple the evaporator/condenser design from the performance by showing the dependence of Bot-PTES

efficiencies on ΔTcold. This process is useful when comparing against other designs, such as a water-cooled evaporator condenser, where the heat transfer coefficients can be about 16-68 times higher than with an air-cooled design [49].

Although a ΔTcold of 20-25 K is typical for steam bottoming systems, and also used for the proposed baseline design, the economic optimum for a Bot-PTES system may differ. Furthermore, Figure 25 shows that this baseline Bot-PTES system is significantly less efficient than other quoted PTES systems. Other proposed PTES systems have had significantly smaller ΔTcold by designing a Cold TES with higher heat transfer and no auxiliary power requirement (i.e. fan power). For example, the supercritical CO2 PTES system proposed by Mercangoz et al. (2012) uses an ice/water phase change Cold TES in their design to obtain a ΔTcold of about 1-3 K [21]. They predicted their commercial system could obtain about 65% round-trip efficiency.

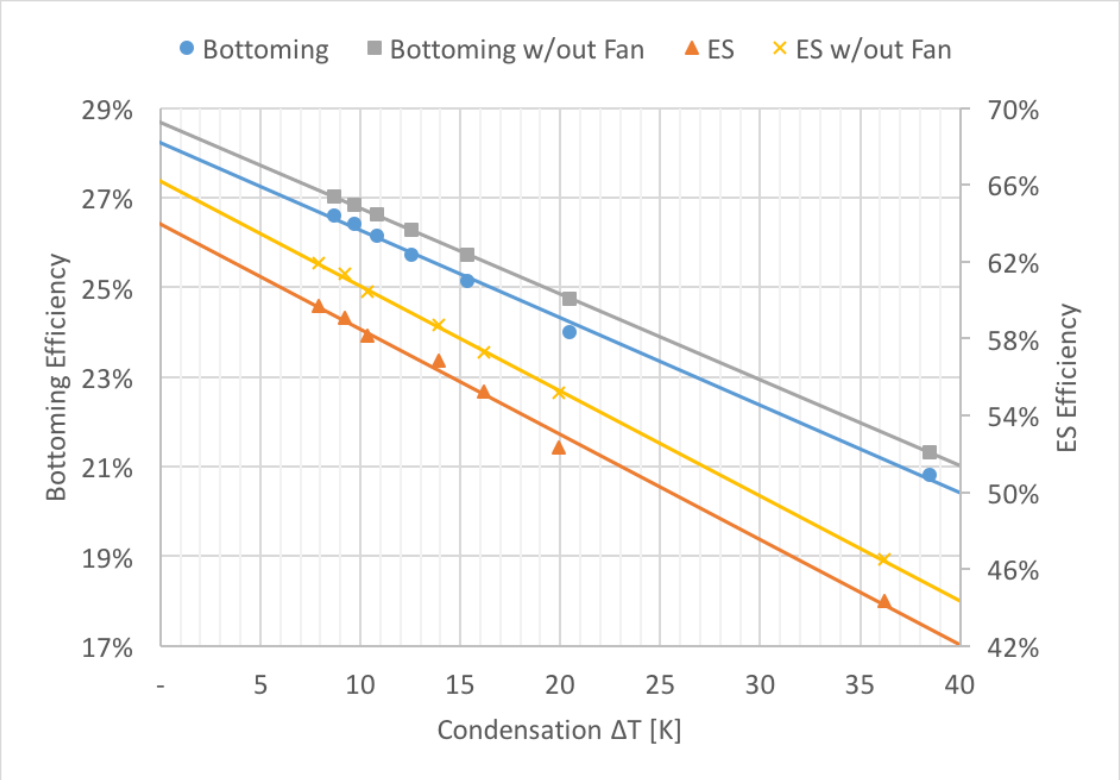

Figure 25: Evaporator/condenser temperature difference performance sensitivity.

3.3.3. Peak Pressure

The peak pressure had significant effects on the performance of both the ES and the bottoming mode operations. Figure 26 shows the overall effect of peak pressure on system efficiency. Similar to a steam bottoming system, this ammonia bottoming system showed higher bottoming efficiency with increased pressure. This improvement in efficiency was due to higher utilization of the high temperature heat from the exhaust gas, as well as reduced heat load on the evaporator/condenser. As pressure was increased, the temperature of the ammonia vapor at the exit of the expander (State 1, Figure 14) decreased during discharge (i.e., less superheat). This lead to more net work out of the system for the same exhaust heat input.

For the ES mode, the absolute ES capacity of the Hot TES was held constant (see $\mathrm{E_{ref}}$ in equation 3.1). With lower peak pressures, the peak temperature in the Hot TES also decreased; therefore, to get the same total heat storage required the Hot TES to be charged/discharged more. This process had a similar effect to lowering the utilization of a system while holding the pressure constant (Figure 21).

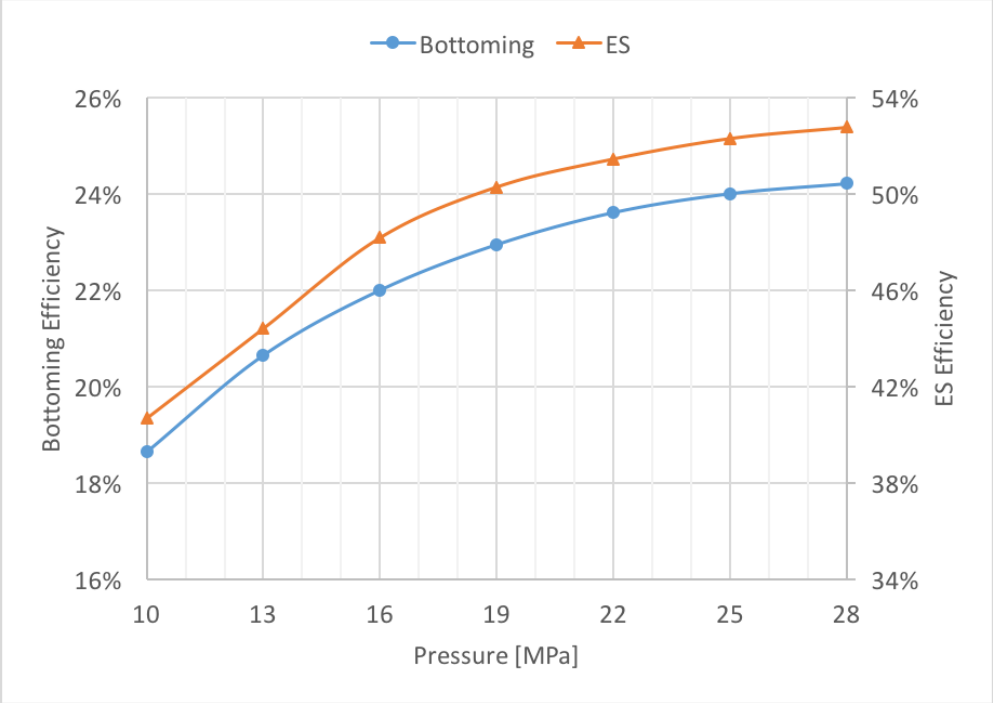

Figure 26: Effect of peak pressure on system efficiencies.

3.3.4. Notes on Frequency Regulation

Frequency regulation is a common application for energy storage systems [59]. Accurate analysis of this system for electric grid frequency regulation during rapidly fluctuating demand requires a dynamic modeling approach, which is outside the scope of this investigation. The results of this study, however, can inform the potential use of this system for this application. For example, it is likely that a system used for frequency regulation would operate well below its maximum power output most of the time, and make the additional capacity available to absorb short, but rapid fluctuations in power.

If the Bot-PTES system oscillates between charge and discharge for short periods of time, then the capacitance of the evaporator/condenser volume can help decrease ΔTcold and the fan use. For example, when the system transitions from charge to discharge, the WF does not change instantaneously from a temperature below ambient to a temperature above ambient within the evaporator/condenser. Instead, the fluid mixes within the evaporator/condenser volume, and the condensation pressure slowly increases over time, leading to a transient variation in evaporation/condensation temperature. During the transient portion, the fan may not be used at all if it is expected that the system will soon transition back to charge to regulate frequency of the grid. Therefore, an efficiency close to 0 K temperature difference with no fan in Figure 25 (~66%) may approximate the ES system in frequency regulation mode.

3.4. Coupling Bottoming and ES Analysis

After evaluating the Bot-PTES system separately as a bottoming system and as an ES system, an evaluation of a combined system was also performed.

There are many tradeoffs to consider when using a single system for two different functions. For example, there are finite hours in a day, and finite power, which can be consumed or generated by the system. This section covers one example of how such a system could be implemented, as explained in the analysis methods section, and the performance that can be expected from such a system.

The coupled Bot-PTES efficiency results are summarized in Table 9. Notice that the bottoming efficiency assumed in this example was the same achieved by the stand-alone bottoming mode operation (Table 8).

Gross ES efficiency ($\eta_{\mathrm{ES,gross}}$)	125.6%
Effective bottoming efficiency (η^{*}_{Bot})	24.0%
Effective ES efficiency ($\eta_{\mathrm{ES,effective}}$)	57.6%
Stand-alone ES efficiency (η_{RT})	58.1%
Total time of operation [hours]	19.0

Table 9: Coupled bottoming with ES efficiency results.

The synergistic functionality of Bot-PTES enables it to achieve 125.6% gross ES efficiency when operating in this nominal mode. In a way, the Bot-PTES system can be viewed as an ES system utilizing heat to improve its performance. In this example, the heat input available was quite large: therefore, the Bot-PTES system generated net power while storing energy from the grid.

The effective ES efficiency ($\eta_{\mathrm{ES,effective}}$) was then calculated and compared to stand-alone ES operation under the same power inputs. The stand-alone ES efficiency operating with 40% of nominal mass flow during charge and 66.7% nominal mass flow in discharge gives 58.1% ES efficiency. When assuming an equivalent 24.0% bottoming efficiency for the coupled operation, the energy balance shows an effective ES efficiency of 57.6%--only 0.5% different than stand-alone operation. Therefore, for the case presented, there is effectively negligible change in efficiency for coupled operation compared to stand-alone operation.

3.5. Levelized Cost of Energy

A range of expected performance parameters was used for the integrated Bot-PTES system to compare it to other technologies in terms of LCOE. The range of values implemented for the Bot-PTES system, as well as other two other typical ES systems—Compressed Air Energy Storage (CAES) and lithium-ion batteries—are shown in Table 10. Hours in this table represent hours at nominal (rated) power. The bottoming power factor is the relative system power in bottoming mode relative to ES discharge mode. When a range of values is shown, the first value

coincides with the lowest LCOE in the range, while the second value coincides with the highest LCOE in the range. It was assumed that no tax credits were given for the ES system.

	Bot-PTES	CAES	Lithium-Ion
Installed Capital Energy Cost [$/kWh]	157	30	444
Installed Capital Power Cost [$/kW]	1303	1336	0
Storage Capacity [hours]	4	4	4
Fixed O&M [$/kW/year]	6	6	10
Variable O&M [$/MWh]	2.75	0	0
Average Stand-Alone ES Efficiency [%]	52 - 66	75	93
Average Bottoming Power Factor	1.1	N/A	N/A
Storage Capacity [hours]	6 - 4	6 - 4	6 - 4
Average Hours of ES Discharge per Day	5.4-3.6	5.4-3.6	5.4-3.6
Average Hours of Bottoming per Day	10 - 2.4	N/A	N/A
Charge Cost of Energy ($LCOE_R$) [$/MWh]	32-50	32-50	32-50

Table 10: Assumed values for LCOE's of the analyzed ES systems.

In Table 10, the overall installed capital costs were split between energy cost ($/kWh) and power costs ($/kW). The current capital cost estimation for an installed Bot-PTES system by Bright Energy Storage Technologies LLP is $157/kWh for energy-related components and $1303/kW for power-related components. The costs listed for lithium-ion batteries were obtained from Lazard [60]. The costs for CAES were derived from Lazard's estimate of an overall capital cost of $197/kWh for 8 hours by assuming the energy-related costs for CAES are $30kWh.

The LCOE of renewables were selected as $32-50/MWh. The low end of $32/MWh charging cost was obtained from Lazard's lowest calculated LCOE of wind power [55], and $50/MWh was from Lazard's own energy storage LCOE analysis [60].

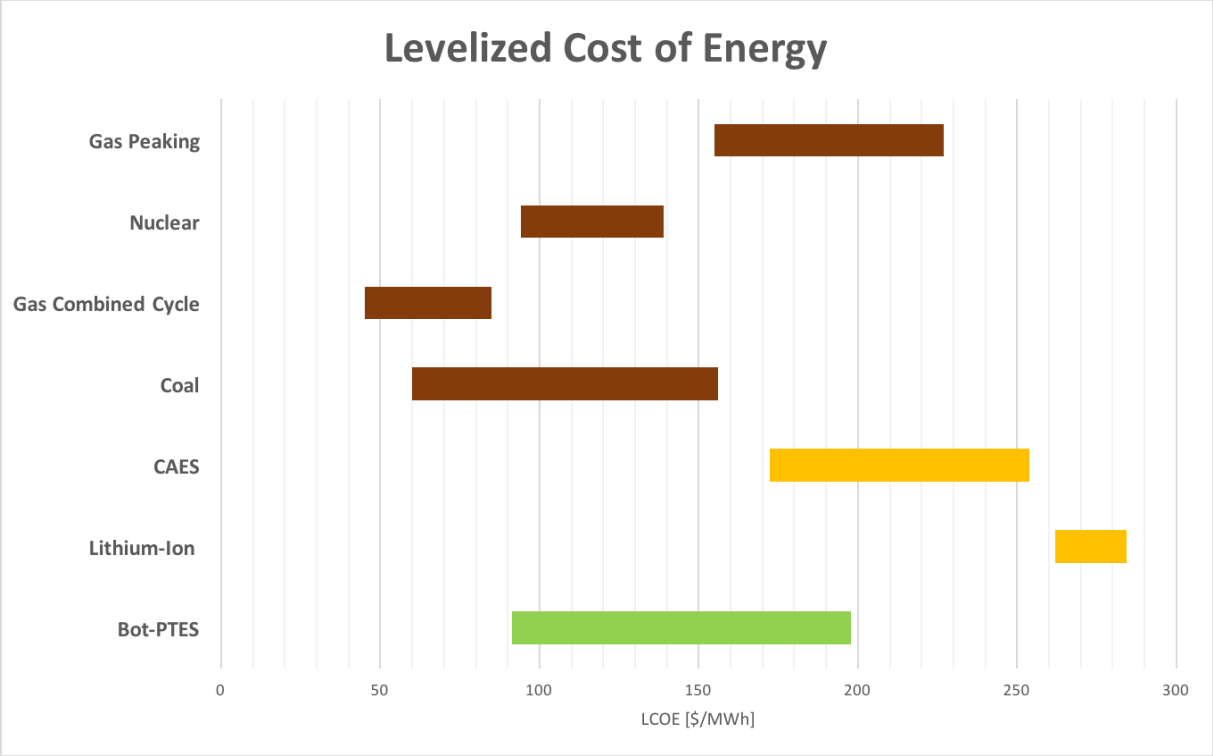

Figure 27: Predicted LCOE of various ES options (orange and green) along with Lazard's LCOE for conventional generation (brown) as of November 2015.

A comparison of the LCOE's of conventional sources and ES systems integrated with renewable energy plants is shown Figure 27. The wide Bot-PTES LCOE range shown on this figure is mostly due to the wide range of potential hours of bottoming per day (2.4 to 10). While the example application presented in this paper assumed four hours of bottoming, a wider range of options was used to generate Figure 27 to show the economic incentive to run more hours per day.

The Bot-PTES system is generally competitive with CAES and most forms of conventional generation, and much better than battery systems for the estimated performance and cost parameters. CAES is widely considered one of the lowest-cost options for utility-scale energy storage, but it uses underground caverns for storage, limiting its implementation [61]. Bot-PTES is particularly competitive with coal generation, which emits the most carbon-dioxide emissions of any system [26]. As fossil fuel prices increase, and government incentives for energy storage become available, the competitiveness of Bot-PTES will improve.

4. Chapter 4: Conclusions

The results presented here provide expected baseline performance for the proposed Bot-PTES system. The baseline Bot-PTES system as a stand-alone ES system and a stand-alone bottoming system is less efficient when compared to other state-of-the-art technology. The proposed baseline Bot-PTES system is relatively inefficient and highlights the challenge of designing one system to do two functions. Nevertheless, the dual-functionality of the Bot-PTES is its greatest strength economically, as shown by the Bot-PTES LCOE when compared to other ES systems. The fundamental advantage of the Bot-PTES system is that it can operate more hours per day (high capacity factor) compared to other energy storage systems, which in turn leads to more revenue generation on the capital investment.

While the results presented here seem to favor using the Bot-PTES system solely as a bottoming system, the combined system has important advantages. Peaker plants are designed for quick, on-demand capacity only during times of peak power demand. They typically do not include a bottoming system because they do not operate enough to justify the capital costs that would be incurred. Bottoming systems are the most expensive (per unit power) and slowest component of a combined-cycle plant. The integrated Bot-PTES system, on the other hand, is able to run more time generating more revenue and is also significantly more responsive than a typical bottoming system. This improved responsiveness is possible because there is constant heat available in the Hot TES ready for use, while conventional bottoming systems require the heat flow to run through the natural gas plant before reaching the steam evaporator.

The analysis presented here is an initial investigation of the potential of Bot-PTES. More detailed analyses are necessary to better understand the potential performance and cost of such a system. More complex system configurations should be investigated, as well as alternate waste heat harvesting applications. The results presented here, however, show a promising option for lower-cost utility-scale energy storage, which could enable higher penetration of renewable energy sources onto the grid.

5. Bibliography

[1] Q. Zhu, High-efficiency power generation – review of alternative systems, 2015.

[2] M.F. Uber, ein neues Verfahren zur Aufspeicherung elektrischer Energie, Mitteilungen Der Vereinigung Der Elektrizitätswerke. 354 (1924) 27–35.

[3] M.F. Das, thermodynamische Speicherverfahren von Marguerre, Escher-Wyss Mitteilungen. 6 (1933) 67–76.

[4] R.P. Cahn, THERMAL ENERGY STORAGE BY MEANS OF REVERSIBLE HEAT PUMPING, US4089744, 1977.

[5] R.P. Cahn, E.W. Nicholson, THERMAL ENERGY STORAGE BY MEANS OF REVERSIBLE HEAT PUMPING UTILIZING INDUSTRIAL WASTE HEAT, US4110987, 1978.

[6] J. Hemrle, L. Kaugmann, M. Mercangoez, Thermoelectric energy storage system with an intermediate storage tank and method for storing thermoelectric energy, US20120080168, 2012.

[7] M. Mercangoez, J. Hemrle, L. Kaugmann, Thermoelectric energy storage system having an internal heat exchanger and method for storing thermoelectric energy, US20120222423, 2012.

[8] J. Hemrle, L. Kaufmann, M. Mercangoez, C. Ohler, Thermoelectric energy storage system and method for storing thermoelectric energy, US20130087301 A1, 2013.

[9] J. Hemrle, L. Kaugmann, M. Mercangoez, A. Z'graggen, Thermoelectric energy storage system with an evaporative ice storage arrangement and method for storing thermoelectric energy, 2012.

[10] J. Hemrle, L. Kaufmann, M. Mercangoez, A. Z'graggen, Electro-thermal energy storage system and method for storing electro-thermal energy, WO2014027093 A1, 2014.

[11] J.S. Howes, J. MacNaghten, Apparatus for storing energy and method of operating an energy storage system comprising such an apparatus, WO2013164562 A1, 2013.

[12] J.S. Howes, J. MacNaghten, Energy storage, US8656712 B2, 2014.

[13] J.S. Howes, J. MacNaghten, R.G. Hunt, Thermal storage system, US20140008033, 2014.

[14] J. MacNaghten, Energy storage apparatus and method of operation of an energy storage system, WO2013164563 A1, 2013.

[15] S. Krause, F. Linder, Waermespeichersystem with combined heat storage, US5269145 A, 1993.

[16] Y.-M. Kim, D.-G. Shin, S.-Y. Lee, D. Favrat, Isothermal transcritical CO2 cycles with TES (thermal energy storage) for electricity storage, Energy. 49 (2013) 484–501. doi:10.1016/j.energy.2012.09.057.

[17] T. Desrues, J. Ruer, P. Marty, J.F. Fourmigué, A thermal energy storage process for large scale electric applications, Appl. Therm. Eng. 30 (2010) 425–432. doi:10.1016/j.applthermaleng.2009.10.002.

[18] J. Howes, Concept and Development of a Pumped Heat Electricity Storage Device, Proc. IEEE. 100 (2012) 493–503. doi:10.1109/JPROC.2011.2174529.

[19] W.D. Steinmann, The CHEST (Compressed Heat Energy STorage) concept for facility scale thermo mechanical energy storage, Energy. 69 (2014) 543–552. doi:10.1016/j.energy.2014.03.049.

[20] H. Jaroslav, K. Lilian, O. Christian, Thermoelectric Energy Storage based on Transcritical

CO 2 Cycle, (2011) 2–6.
[21] M. Mercangöz, J. Hemrle, L. Kaufmann, A. Z'Graggen, C. Ohler, Electrothermal energy storage with transcritical CO2 cycles, Energy. 45 (2012) 407–415. doi:10.1016/j.energy.2012.03.013.
[22] M. Morandin, F. Maréchal, M. Mercangöz, F. Buchter, Conceptual design of a thermo-electrical energy storage system based on heat integration of thermodynamic cycles – Part A: Methodology and base case, Energy. 45 (2012) 375–385. doi:10.1016/j.energy.2012.03.031.
[23] M. Morandin, F. Maréchal, M. Mercangöz, F. Buchter, Conceptual design of a thermo-electrical energy storage system based on heat integration of thermodynamic cycles – Part B: Alternative system configurations, Energy. 45 (2012) 386–396. doi:10.1016/j.energy.2012.03.033.
[24] R. Fauci, B. Heimbach, E. Kaffe, F. Kienzle, L. Kung, FEASIBILITY STUDY OF AN ELECTROTHERMAL ENERGY STORAGE IN THE CITY OF ZURICH, in: 22nd Int. Conf. Electr. Distrib., 2013.
[25] H. Spliethoff, Power Generation from Solid Fuels, 2010. doi:10.1007/s13398-014-0173-7.2.
[26] P. Breeze, Coal-Fired Power Plants, in: Power Gener. Technol., 2nd ed., Elsevier, 2014: pp. 29–65. doi:10.1016/B978-1-4377-7842-7.00006-4.
[27] D. Aquaro, M. Pieve, High temperature heat exchangers for power plants: Performance of advanced metallic recuperators, Appl. Therm. Eng. 27 (2007) 389–400. doi:10.1016/j.applthermaleng.2006.07.030.
[28] H. Chen, D.Y. Goswami, E.K. Stefanakos, A review of thermodynamic cycles and working fluids for the conversion of low-grade heat, Renew. Sustain. Energy Rev. 14 (2010) 3059–3067. doi:10.1016/j.rser.2010.07.006.
[29] H.A. Mlcak, An Introduction to the Kalina Cycle, in: Proc. Int. Jt. Power Gener. Conf., 1996: pp. 1–11.
[30] R. Vasquez Padilla, A. Ramos Archibold, G. Demirkaya, S. Besarati, D. Yogi Goswami, M.M. Rahman, E.L. Stefanakos, Performance Analysis of a Rankine Cycle Integrated With the Goswami Combined Power and Cooling Cycle, J. Energy Resour. Technol. 134 (2012) 032001. doi:10.1115/1.4006434.
[31] G. Demirkaya, R.V. Padilla, D.Y. Goswami, A review of combined power and cooling cycles, Wiley Interdiscip. Rev. Energy Environ. 2 (2013) 534–547. doi:10.1002/wene.75.
[32] J. Ciferno, Pulverized Coal Oxycombustion Power Plants Volume 1 : Bituminous Coal to Electricity Final Report, 2007.
[33] L. Doerte, S.W. Tamme, R. Wörner, A. Zunft, 特约文章 Advances in thermal energy storage development at the German Aerospace Center (DLR), (2012).
[34] W.-C. Choi, H.-D. Yun, C.-G. Cho, L. Feo, Attempts to apply high performance fiber-reinforced cement composite (HPFRCC) to infrastructures in South Korea, Compos. Struct. 109 (2014) 211–223. doi:10.1016/j.compstruct.2013.10.027.
[35] N.N. Htun, S. Sukchai, S. Hemavibool, Properties of Concrete Material for Thermal Energy Storage, (2014) 19–21.
[36] E. John, M. Hale, P. Selvam, Concrete as a thermal energy storage medium for

thermocline solar energy storage systems, Sol. Energy. 96 (2013) 194–204. doi:10.1016/j.solener.2013.06.033.
[37] M. Wu, M. Li, C. Xu, Y. He, W. Tao, The impact of concrete structure on the thermal performance of the dual-media thermocline thermal storage tank using concrete as the solid medium, Appl. Energy. 113 (2014) 1363–1371. doi:10.1016/j.apenergy.2013.08.044.
[38] M. Medrano, A. Gil, I. Martorell, X. Potau, L.F. Cabeza, State of the art on high-temperature thermal energy storage for power generation. Part 2—Case studies, Renew. Sustain. Energy Rev. 14 (2010) 56–72. doi:10.1016/j.rser.2009.07.036.
[39] D. Laing, W.-D. Steinmann, M. Fiß, R. Tamme, T. Brand, C. Bahl, Solid Media Thermal Storage Development and Analysis of Modular Storage Operation Concepts for Parabolic Trough Power Plants, J. Sol. Energy Eng. 130 (2008) 011006. doi:10.1115/1.2804625.
[40] D. Laing, W.-D. Steinmann, R. Tamme, C. Richter, Solid media thermal storage for parabolic trough power plants, Sol. Energy. 80 (2006) 1283–1289. doi:10.1016/j.solener.2006.06.003.
[41] M.N. Strasser, R.P. Selvam, A cost and performance comparison of packed bed and structured thermocline thermal energy storage systems, Sol. Energy. 108 (2014) 390–402. doi:10.1016/j.solener.2014.07.023.
[42] S.E. Faus, 10 MWe solar thermal central receiver pilot plant: Thermal storage subsystem evaluation, subsystem activation and controls testing phase, (1983).
[43] B.M. Brown, M.N. Strasser, R.P. Selvam, Development of a structured thermocline thermal energy storage system, in: World Renew. Energy Forum, WREF 2012, Incl. World Renew. Energy Congr. XII Color. Renew. Energy Soc. Annu. Conf., 2012.
[44] S. Quoilin, I. Bell, A. Desideri, P. Dewallef, V. Lemort, Methods to increase the robustness of finite-volume flow models in thermodynamic systems, Energies. 7 (2014) 1621–1640. doi:10.3390/en7031621.
[45] C. Schulze, M. Graber, W. Tegethoff, A Limiter for Preventing Singularity in Simplified Finite Volume Methods, in: MATHMOD 2012 7th Vienna Int. Conf. Math. Model., International Federation of Automatic Control, 2012.
[46] S. Quoilin, A. Desideri, J. Wronski, I. Bell, V. Lemort, ThermoCycle : A Modelica library for the simulation of thermodynamic systems, (2014). doi:10.3384/ECP14096683.
[47] B. Xu, P. Li, C.L. Chan, Extending the validity of lumped capacitance method for large Biot number in thermal storage application, Sol. Energy. 86 (2012) 1709–1724. doi:10.1016/j.solener.2012.03.016.
[48] V. Gnielinski, On heat transfer in tubes, Int. J. Heat Mass Transf. 63 (2013) 134–140. doi:10.1016/j.ijheatmasstransfer.2013.04.015.
[49] F.P. INCROPERA, D.P. DEWITT, T.L. BERGMAN, A.S. LAVINE, Introduction to Heat Transfer, John Wiley & Sons, Inc., 2007.
[50] Y. Cengel, Introduction to Thermodynamics and Heat Transfer, 2nd ed., McGraw Hill, 2008.
[51] A.M. Jacobi, Heat Transfer to Air-Cooled Heat Exchangers, in: Eng. Data B. III, 2005.
[52] C.C. Wang, Y.J. Chang, Y.C. Hsieh, Y.T. Lin, Sensible heat and friction characteristics of plate fin-and-tube heat exchangers having plane fins, Int. J. Refrig. 19 (1996) 223–230. doi:10.1016/0140-7007(96)00021-7.
[53] T. Fout, A. Zoelle, D. Keairns, M. Turner, M. Woods, N. Kuehn, V. Shah, V. Chou, L.

Pinkerton, Cost and Performance Baseline for Fossil Energy Plants, 2015. doi:DOE/NETL-2010/1397.
[54] F-Class 7F.04 Gas Turbine (60Hz), 2015.
[55] Lazard Ltd, Lazard's Levelized Cost of Energy Analysis - Version 9.0, 2015. http://www.lazard.com/.
[56] National Energy Technology Laboratory, Power Systems Financial Model Version 6.6 User's Guide, Power. (2011).
[57] J. Mctigue, A. White, C.N. Markides, Parametric studies and optimisation of pumped thermal electricity storage, Appl. Energy. 137 (2015) 1–24. doi:10.1016/j.apenergy.2014.08.039.
[58] R. Tamme, Concrete Storage : Update on the German concrete TES Program, Golden, CO, 2003. http://www.nrel.gov/csp/troughnet/pdfs/tamme_concrete_storage.pdf.
[59] S. Koohi-Kamali, V.V. Tyagi, N. a. Rahim, N.L. Panwar, H. Mokhlis, Emergence of energy storage technologies as the solution for reliable operation of smart power systems: A review, Renew. Sustain. Energy Rev. 25 (2013) 135–165. doi:10.1016/j.rser.2013.03.056.
[60] Lazard Ltd, Lazard's levelized cost of storage analysis — version 1.0, Lazard. (2015).
[61] J.E. Mason, C.L. Archer, Baseload electricity from wind via compressed air energy storage (CAES), Renew. Sustain. Energy Rev. 16 (2012) 1099–1109. doi:10.1016/j.rser.2011.11.009.